Nanoscale Advances

ROYAL SOCIETY OF CHEMISTRY

REVIEW

View Article Online
View Journal | View Issue

Check for updates

Cite this: *Nanoscale Adv.*, 2020, **2**, 1792

Comprehensive understanding of the synthesis and formation mechanism of dendritic mesoporous silica nanospheres

Pan Hao,† Bo Peng,† Bing-Qian Shan, Tai-Qun Yang * and Kun Zhang *

The interest in the design and controlled fabrication of dendritic mesoporous silica nanospheres (DMSNs) emanates from their widespread application in drug-delivery carriers, catalysis and nanodevices owing to their unique open three-dimensional dendritic superstructures with large pore channels and highly accessible internal surface areas. A variety of synthesis strategies have been reported, but there is no basic consensus on the elucidation of the pore structure and the underlying formation mechanism of DMSNs. Although all the DMSNs show a certain degree of similarity in structure, do they follow the same synthesis mechanism? What are the exact pore structures of DMSNs? How did the bimodal pore size distributions kinetically evolve in the self-assembly? Can the relative fractions of small mesopores and dendritic large pores be precisely adjusted? In this review, by carefully analysing the structures and deeply understanding the formation mechanism of each reported DMSN and coupling this with our research results on this topic, we conclude that all the DMSNs indeed have the same mesostructures and follow the same dynamic self-assembly mechanism using microemulsion droplets as super templates in the early reaction stage, even without the oil phase.

Received 18th March 2020
Accepted 16th April 2020

DOI: 10.1039/d0na00219d

rsc.li/nanoscale-advances

Open Access Article. Published on 16 April 2020. Downloaded on 2/9/2026 9:27:09 AM.
This article is licensed under a Creative Commons Attribution-NonCommercial 3.0 Unported Licence.

1. Introduction

The high porosity and accessible surface modification of bulk mesoporous silica (in particular MCM-41 and SBA-15, two kinds of ordered mesoporous materials)[1–3] have opened a new route to the formation of porous supports with high performance catalysts and a potential platform for advanced biomolecule carriers for targeted and controlled drug delivery systems.[4,5] Because the liquid crystal templating (LCT) principle of the synthesis is quite simple, a variety of sol–gel processes have been developed to synthesize ordered mesostructured silica frameworks with highly tunable porosities and morphologies using varied surfactants as templates including cationic, anionic and

Shanghai Key Laboratory of Green Chemistry and Chemical Processes, College of Chemistry and Molecular Engineering, East China Normal University, Shanghai, P. R. China. E-mail: tqyang@chem.ecnu.edu.cn; kzhang@chem.ecnu.edu.cn; Fax: +86-21-62232753; Tel: +86-21-62232753

† P. H. and B. P. equally contributed to this research.

Bo Peng obtained his BS degree from Donghua University in 2017. He is currently a PhD student in the Shanghai Key Laboratory of Green Chemistry and Chemical Processes at East China Normal University under the supervision of Prof. Kun Zhang. His research interests focus on the synthesis and mechanistic understanding of mesoporous materials and their application in nanocatalysis.

Taiqun Yang received his BS (2012) from Xi'an Jiaotong University and PhD (2017) from East China Normal University. He is now a postdoctoral researcher at East China Normal University working with Prof. Kun Zhang and Prof. Peng Wu. His research interests focus on synthesis and characterization of luminescent nanomaterials, including metal nanocluster, graphene and perovskite quantum dots. His research mainly focuses on the ultrafast electron/phonon dynamics during the photoemission process.

This journal is © The Royal Society of Chemistry 2020

Open Access Article. Published on 16 April 2020. Downloaded on 2/9/2026 9:27:09 AM.
This article is licensed under a Creative Commons Attribution-NonCommercial 3.0 Unported Licence.

nonionic surfactants.[6–8] Thus, the past three decades have witnessed the rapid development of mesoporous silica materials with diverse topologies and architectures.

Due to very short diffusion length and large pore size, mesoporous silica nanoparticles (MSNs) attracts much more research interests in the fields of nanocatalysis and drug delivery.[9–15] The sol–gel soft-templating synthesis of MSNs is the best and easiest method and was first reported by the groups of Cai,[16] Mann[17] and Ostafin.[18] Then the term MSNs was popularized by Victor Lin to represent mesoporous silica nanospheres.[5,19–22] Subsequently, the groups of Bein,[23–26] Mou,[27–29] Tatsumi[30–33] and Kuroda[34–39] followed this line to carry out extensive research. Several important reviews written by some of them cover different aspects of mesoporous silica nanoparticles, such as preparation, characterization, formation mechanism, and applications (in particular targeted drug delivery systems), and are available in the literature.[5,9,20–22,40–49] It is worth noting that without the addition of the micelle organic swelling agents, the common surfactant templated MSNs have pores smaller than 3.0 nm,[50] which significantly limits their wide use as metal nanoparticles, enzyme immobilizing supports, and multifunctional drug delivery nanocarriers. Therefore, an enlargement of their mesopore size is desired to extend their applications in different fields. Consequently, the scientific community started to look for a new generation of mesoporous materials with both a short diffusion length and wide pores aimed at improved accessibility and molecular transport.

In this line of thinking, DMSNs with unique open three-dimensional dendritic superstructures (in some cases, also called hierarchical pore systems) have intensively been developed and have attracted rapidly growing attention since the 2010s. Compared with conventional MSNs with two dimensional hexagonal ordered mesopores (pore symmetry: *p6mm*) and uniform pore sizes, DMSNs have unique three-dimensional disordered superstructures with many permeable center-radial large pore channels and high pore volumes.[51–54] So far, corresponding to synthetic systems, several terms have been used to describe their morphology such as fibrous, nanoflowers, radial wrinkle structured, stellar shaped, *etc.* The different morphological terminologies used indeed indicate that the mesostructures and formation mechanism of DMSNs have not been fully revealed. Since the intrinsic branching architecture of DMSNs is reminiscent of natural mineral dendrimers and artificial organic dendrimers, the nomenclature of dendritic mesoporous silica nanospheres could be well-accepted (Fig. 1).[55–58] However, there exists an urgent need to compare the various methods for their preparation, not least to describe in detail the properties of the materials as well as to establish a firm link between the structure and function. In this report, based on our continuous and long-term studies in the past decade, we summarize recent findings on this topic and the content of this review is organized as follows: the emergence and evolution of DMSNs are first discussed in a brief introduction; in the second section, we present the state-of-the-art progress in the strategies for preparing DMSNs, with emphasis on the elucidation of the mesostructural characteristics and physicochemical properties of DMSNs. In addition, by carefully analyzing the structure and synthetic mechanism of each reported DMSN, combined with our studies on this topic, all the syntheses of DMSNs in the documented records are systematically classified into three main groups, including the micro-emulsion templating (MET) approach, the organosilane assisted co-condensation (OAC) method and the spherical micelle self-aggregated assembly (SMSAA) strategy, and the simplest and most reproducible preparation method for the DMSNs is highlighted by comparing the advantages and disadvantages of each method; in the third part, several typical examples are presented to show the unique nanoconfinement effect of spherical mesopores in DMSNs, which could be used as an ideal nanoreactor or platform for the preparation of highly efficient heterogeneous nanocatalysts and the fabrication of photoluminescent (PL) materials. Most interestingly, in this part, by clustering of nonconjugated organic functional groups in the spherical mesopores of DMSNs, the first PL MSNs with tunable colors and high quantum yield (QE) were reported using a simple post-grafting technique in the absence of metals, which completely subverts one's understanding on the origin of the photoluminescence emission of metal nanoclusters (NCs) and other related quantum dots. Last, but not least, opinions and challenges for the future progress of these materials are addressed. We sincerely expect that this summary and in-depth discussion on the formation mechanism of DMSNs could give materials scientists and chemists more inspiration to accelerate the DMSN family's booming development in related interdisciplinary research.

Kun Zhang was born in Shangdong (Gaomi), China, and received his PhD from the École Normale Supérieure de Lyon (ENS-Lyon), France, in 2008. Then he joined the East China Normal University as an assistant professor, and he was very quickly promoted to associate professor and full professor in 2011 and 2015. He was also a visiting professor at ENS-Lyon in 2014, 2016 and 2018. In current research projects, we are trying to develop new methodologies in order to precisely control the nanostructure of porous materials and find out a method to apply them in heterogeneous catalysis.

2. Typical synthetic strategies of DMSNs

Differing from the synthesis of MCM-41 with ordered mesostructures, the preparation of DMSNs is complex, and the conventional soft-templating methods are not suitable due to the complex dynamic self-assembly of negative silicate species

Open Access Article. Published on 16 April 2020. Downloaded on 2/9/2026 9:27:09 AM.
This article is licensed under a Creative Commons Attribution-NonCommercial 3.0 Unported Licence.

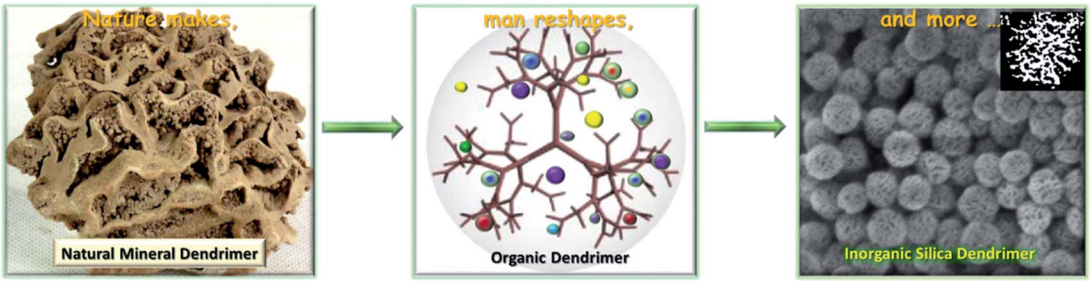

Fig. 1 Schematic illustration of dendritic mesoporous silica nanospheres (DMSNs) with the unique branching architecture, which is reminiscent of natural mineral dendrimers and artificial organic dendrimers.

and surfactants on the molecular scale. So far, more than 20 synthetic methods have been reported to synthesize the DMSNs with a 3D center radial pore structure. According to the common characteristics of their syntheses, whether an oil-phase organosilane reagent is used, they are classified into three main categories and also are summarized in Table 1:

(1) The micro-emulsion templating (MET) approach, also called the biphase stratification approach, emphasizing the self-assembly of silicate species with a surfactant at the interface of the immiscible phases of water and oil.

(2) The srganosilane assisted co-condensation (OAC) method, featuring the use of custom-tailored organotrialkoxysilane with special organic functional groups.

(3) The simplest and most reproducible spherical micelle self-aggregated assembly (SMSAA) strategy using a conventional cationic surfactant, free of any organic additives.

2.1. Micro-emulsion templating approach

Because of the variety and ease of control, the substructures of microemulsions were used as templates to control the synthesis of mesoporous silica materials with different morphologies and mesostructures. In 2008, Okuyama and his coworkers first reported the synthesis of spherical mesoporous silica particles with a tunable pore size and tunable outer particle diameter in the nanometer range in a water/oil phase using the cationic surfactant CTABr as a template (Fig. 2a and b).[59] This method involves the simultaneous hydrolytic condensation of tetraethylorthosilicate to form silica and polymerization of styrene into polystyrene (PS) in the presence of octane as the oil phase, and subsequent removal of PS by high temperature calcination in air resulted in the formation of DMSNs with large pores, where PS beads actually act as hard templates (Fig. 2c). By varying the conditions of the dispersed phase, *e.g.*, the ratio of octane/water, the styrene concentration, the pH, and the temperature, during preparation, the pore size (4–15 nm) and grain diameter (20–80 nm) of the prepared MSNs can be precisely tuned. However, further research performed by Holmberg[60] suggested that the MSNs synthesized under the same conditions free of styrene possessed the same mesostructures (Fig. 2d and e), indicating that the polystyrene (PS) beads formed by polymerization of styrene were not the only template for the formation of DMSNs with large pores. In turn, the authors concluded that the microemulsion spontaneously formed at the interface of water and oil played the main role in controlling the formation of DMSNs with hierarchical pores (Fig. 2f). This conclusion was further supported by the subsequent research of Ernawati and his coworkers.[61]

Table 1 Summary of synthetic strategies and physical properties of various DMSNs

Synthetic strategy	Main feature	Solvent	Particle size (nm)	Pore size (nm)	S_{BET}[a] (m^2 g^{-1})	V_t[b] (mL g^{-1})	Ref.
Oil–water mixed micro-emulsion templating (MET) approach, also called the biphase stratification approach[51,59–90]	The interfacial assembly occurs at the oil–water biphase interface	Octane	20–80	4–15	600	1.0–1.5	59
		Cyclohexane	250–450	4.6	641	—	62
		1-Octadecene, decahydronaphthalene, or cyclohexane	110–280	2.8–13.0	<700	0.6–1.7	69
		Ethyl ether	150–600	2.7	1078	1.0	76
		Chlorobenzene	180	45	554	2.59	71
Organosilane assisted co-condensation (OAC) method[91–94]	The interfacial assembly is related to the specific nature of the used organotrialkoxysilane	Water	50	4.0	519	0.25	91
		Water	<70	2.4	953	1.5	92
		Water	30	6.2	614	2.2	93
Spherical micelle self-aggregated assembly (SMSAA) strategy[95–103]	The reaction occurs in the single aqueous phase at pH *ca.* 7	Water	50–300	3.0/15–20	<600	1.4–2.1	95

[a] Specific surface area measured by N_2 physisorption. [b] Total pore volume measured at $P/P_0 = 0.99$.

 This journal is © The Royal Society of Chemistry 2020

Open Access Article. Published on 16 April 2020. Downloaded on 2/9/2026 9:27:09 AM.
This article is licensed under a Creative Commons Attribution-NonCommercial 3.0 Unported Licence.

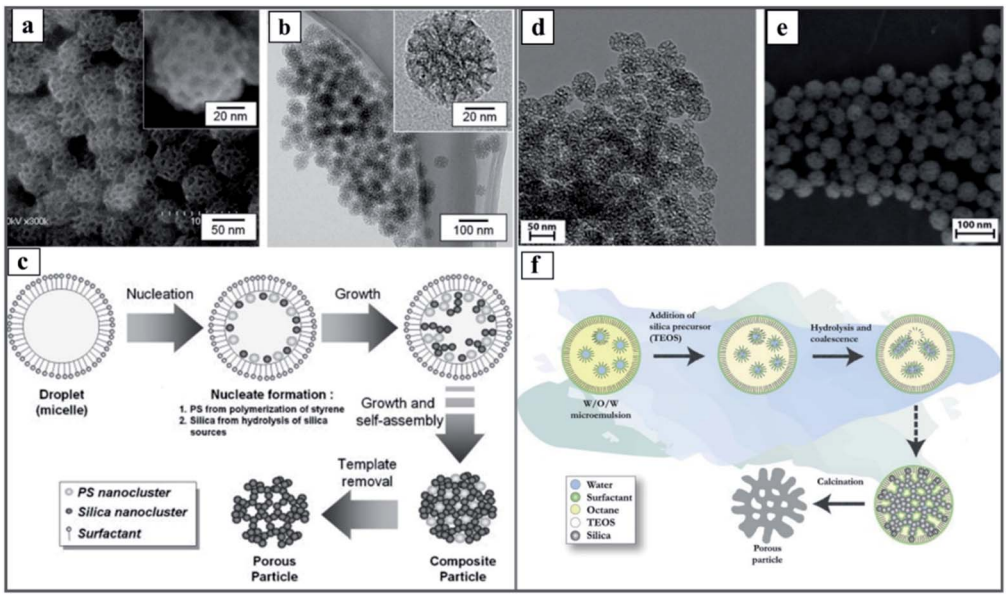

Fig. 2 SEM (a) and TEM (b) images and proposed formation mechanism (c) of mesoporous silica nanoparticles prepared by Okuyama and his coworkers with styrene.[59] Reproduced with permission from ref. 59. Copyright 2009 Elsevier Ltd. And TEM (d) and SEM (e) images and proposed formation mechanism (f) of mesoporous silica nanoparticles prepared by Holmberg without styrene.[60] Reproduced with permission from ref. 60. Copyright 2016 Elsevier Ltd.

Following the same principle of the MET mechanism, but without organic polymer monomers, Polshettiwar and his coworkers reported the synthesis of dendritic silica nanoparticles with fibrous morphologies (or center-radial wrinkle structures) under microwave-assisted hydrothermal conditions, which were named KCC-1,[62] which triggered a boom in the synthesis of DMSNs. But the earlier proposed formation mechanism was too simple to understand (Fig. 3A). More comprehensive studies on the formation mechanism of KCC-1 were carried out by Febriyanti.[66] The morphology of KCC-1 was observed to be a bicontinuous concentric lamellar morphology (Fig. 3B–E) using a sophisticated TEM technique by a detailed comparison of the gray value intensity profiles of the TEM images of different types of MSNs, and it was concluded that the reverse micelle in the reaction media and the polysiloxane species with varied Si–O–Si chain lengths played an important role in the assembly of DMSNs (Fig. 3F). Further in-depth investigations by Polshettiwar and his coworkers showed that the formation of KCC-1 was attributed to the structural evolution of the microemulsion template.[64,65]

Very recently, based on a simple adjustment of the water-surfactant-oil ternary phase diagram, more detailed investigations of the formation mechanism of KCC-1 were elegantly performed by Lee and his coworker following the same recipe as that for KCC-1. Note that the obtained DMSNs herein were named wrinkled silica nanoparticles (WSNs).[67,68] It is well known that the phase behavior of the ternary systems (the so-called "Winsor system") is determined by the surfactant concentration and the Winsor value R, which is a variable depending on temperature, salinity, and affinity of each component. They confirmed that WSNs were preferentially generated in the bicontinuous microemulsion phase of the

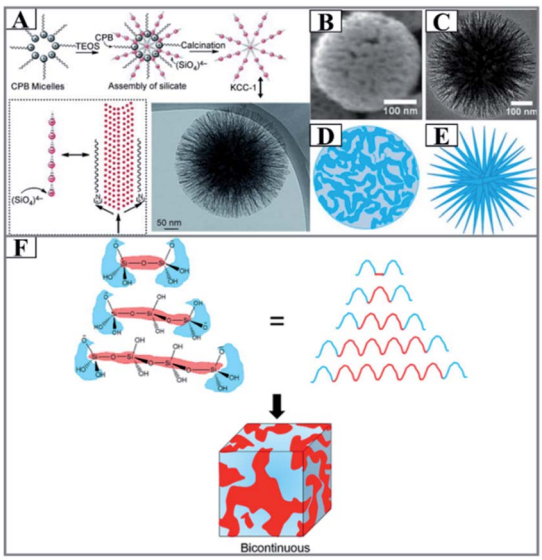

Fig. 3 (A) Schematic of the silica nanosphere (KCC-1) formation proposed by Basset.[62] CPB: cetylpyridinium bromide, TEOS: tetraethyl orthosilicate. Reproduced with permission from ref. 62. Copyright 2010 Wiley-VCH. (B) SEM and (C) TEM images of KCC-1 with their illustrations drawn in (D) and (E), respectively. (F) Self-assembly of the silicate oligomer for the formation of bicontinuous morphology (the ABA silicate oligomer consists of two A blocks (blue) separated by a B block (red), where the A block consists of O–H groups in the terminal and the B block is a Si–O–Si chain of the oligomers. This pattern is similar to that of ABA triblock copolymer chains where A and B blocks are formed from different monomers. When the B blocks of polysiloxane have a range of chain lengths, a bicontinuous structure is formed).[66] Reproduced with permission from ref. 66. Copyright 2016 American Chemical Society.

Open Access Article. Published on 16 April 2020. Downloaded on 2/9/2026 9:27:09 AM.
This article is licensed under a Creative Commons Attribution-NonCommercial 3.0 Unported Licence.

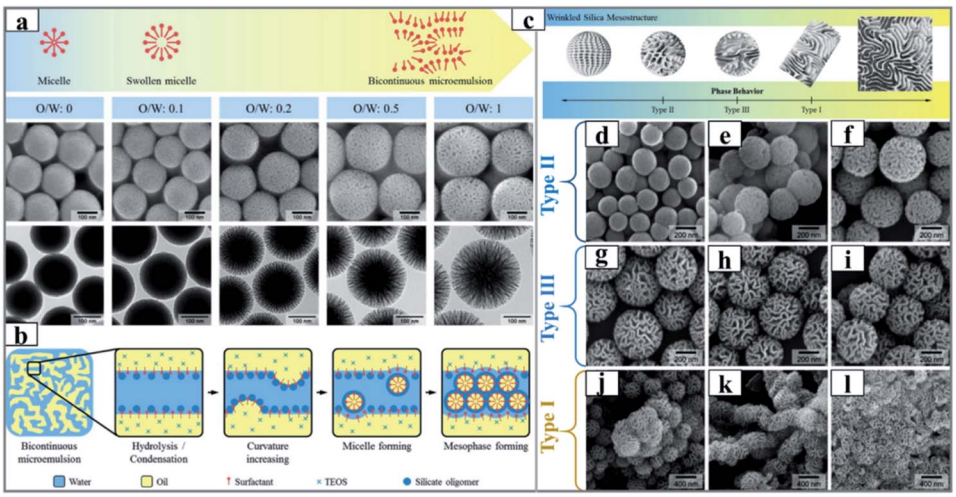

Fig. 4 (a) Schematic (upper panel) and SEM/TEM images (lower panel) of silica nanoparticles synthesized with different volume ratios of cyclohexane to 15 mL of an aqueous solution of urea (0.3 g), CPB (0.5 g) and iso-propanol (0.46 mL), and (b) schematic illustration of the mesophase forming mechanism at the microemulsion interface.[67] Reproduced with permission from ref. 67. Copyright 2012 American Chemical Society. The illustration (c) and SEM images (d–l) of silica-based nanoparticles synthesized from the different biphase regions of Winsor II (a–c),Winsor III (d–f) and Winsor I (g–i), respectively.[68] Reproduced with permission from ref. 68. Copyright 2014 American Chemical Society.

Winsor III system, and that the particle size of the wrinkled silica nanoparticles (WSNs) and the connective morphology of the WSMs can be precisely controlled by deliberately tuning the volume ratio of water/oil with alkyl alcohols as the co-solvent (Fig. 4). In addition, these authors first showed that WSNs intrinsically had a bi-modal pore size distribution with a very sharp peak in the 2–4 nm range and a broad peak in the 15–50 nm range, and the smaller pores were embedded in the wall of WSNs, which was attributed to the emulsion rupture-inversion in the early nucleation process (Fig. 4b), suggesting a completely different formation mechanism from that of classical MCM-41.[104]

Later, Zhao and his collaborators developed a new biphase stratification approach for the synthesis of novel 3D-DMSNs with multigenerational and hierarchical dendrimer-like center-radial mesopore channels (Fig. 5), and it was also successfully expanded to prepare uniform core–shell mesoporous structures with varied functional cores (such as Au nanoparticles and Ag nanotubes) and 3D-dendritic mesopore radial channels.[69] In this report, a sophisticated interfacial

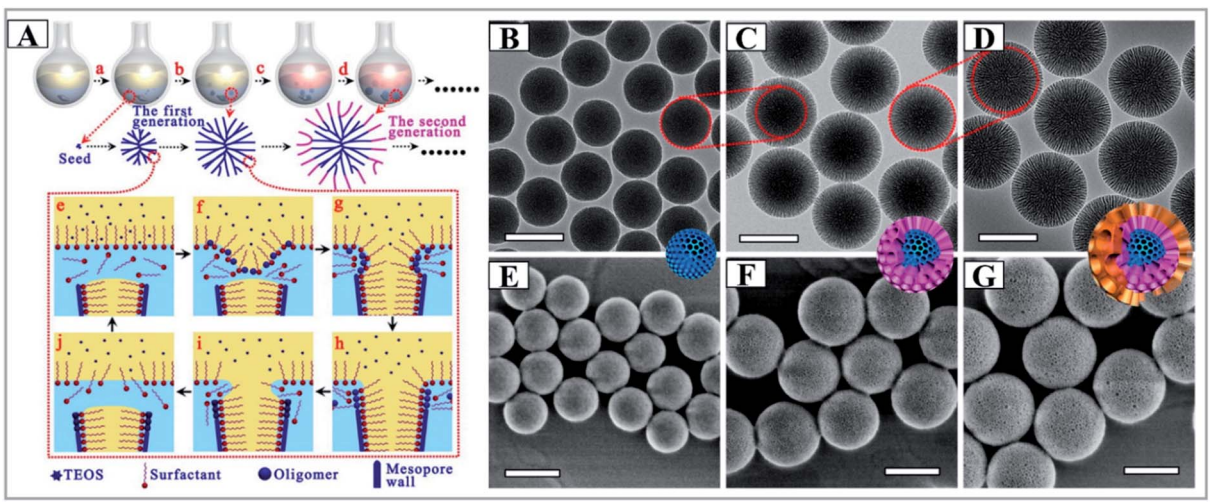

Fig. 5 (A) Synthesis process of the 3D-dendritic MSNSs and the mechanism of interfacial growth, (a) nucleation process of the 3D-dendritic MSNSs; (b) growth process of the first generation of the 3D-dendritic MSNSs; (c) changing the upper oil phase; (d) growth process of the second generation of the 3D-dendritic MSNSs; (e–h) the mechanism of one single mesopore-channel growth with swelling. TEM (B–D) and SEM (E–G) images of the extracted 3D-dendritic MSNSs with one (B and E), two (C and E), and three generations (D and G) prepared *via* the biphase stratification approach. All scale bars in the TEM and SEM images are 200 nm.[69] Reproduced with permission from ref. 69. Copyright 2014 American Chemical Society.

 This journal is © The Royal Society of Chemistry 2020

Open Access Article. Published on 16 April 2020. Downloaded on 2/9/2026 9:27:09 AM.
This article is licensed under a Creative Commons Attribution-NonCommercial 3.0 Unported Licence.

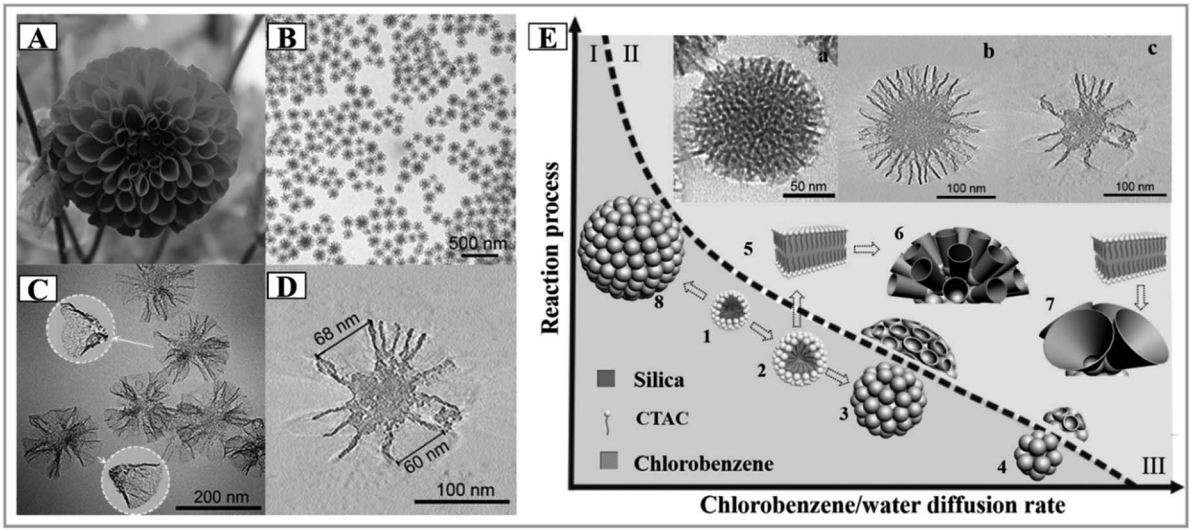

Fig. 6 A picture of a dahlia photographed by C. Xu in Tasmania (A). TEM images at low magnification (B) and high magnification (C), an ET slice (D) and the proposed formation mechanism (E) of MSN-CC.[71] Reproduced with permission from ref. 71. Copyright 2015 Wiley-VCH.

emulsion driven self-assembly mechanism was proposed to explain the nucleation and growth process of DMSNs. Very recently, in the final collected sample, Yu and his coworkers found the presence of isolated cone-shaped structures, which could be used as building subunits to assemble DMSNs, whose shape was reminiscent of the funnel-like shape in the model of the biphase stratification approach (Fig. 6A–D).[71] It is importantly noted that both groups commented that the final mesostructure of DMSNs was sensitive to the stirring rate of reaction media as discussed by other groups,[71,72,88] which indicates the rationality of the MET mechanism.

Indeed, at the time of discovery of mesoporous materials, studies using microemulsion systems as a supertemplate for the synthesis of MSNs were extensively performed, in particular under acidic conditions.[105–107] However, synthesis under alkaline conditions did not attract enough attention except from Cai's group.[73,74,108] By employing a non-stable interface of the biphasic oil–water (OWTP) system and adjusting the molar ratios of oil/water and the alkalinity of the OWTP system using diethyl ether as a co-solvent, Cai and his coworkers first reported the preparation of mesostructured silicas with diversified particle morphologies. By systematic investigation, they established a detailed reaction phase diagram to direct the synthesis of MSNs, and a variety of morphologies of the collected products was reported. In fact, in these studies, one of the obtained nanoparticles (NPs) was first named radiolarian-like mesoporous silica (RMS), analogous to the shape of a coronavirus. Indeed, it is the first example of DMSNs. From the viewpoint of historical evolution, the contribution of Cai and his coworkers in this new rising field has been neglected.[73,74] In addition, in their reports, two common features for the synthesis of DMSNs were also carefully depicted: RMS showed an interesting bi-modal pore size distribution with smaller mesopores (centered at ~3 nm) and larger ones of ~34 nm; its synthesis was very sensitive to the volume ratio of water/diethyl ether and the stirring rate of reaction media.[73,74] These intriguing experimental observations were attributed to the dynamic self-assembly of micelles at the unstable oil–water interface. The subsequent investigations by He and his coworkers further developed this method;[76,109] they noted that the use of diethyl ether with a low boiling point of 34 °C was necessary for the formation of dendritic pores due to ethyl ether gasification.[64] Thereafter, a huge amount of experimental evidence proved that any non-miscible water–oil biphase system was effective for the synthesis of DMSNs, such as toluene,[77] trialkylbenzenes,[78,79] ethyl acetate,[80] *N*,*N*-dimethyldecylamine,[81] benzyl acetate,[82] aldehyde,[83] *etc.*, which evidences the universality of the MET mechanism for the synthesis of DMSNs.

To sum up, water-surfactant-oil ternary systems exhibit various phase behaviors and substructures that depend on their chemical composition and component ratio, the substructures of which can be used as super-templates for the synthesis of DMSNs. The MET mechanism provides an example for constructing hierarchical porous silica NPs with varied morphologies and tunable mesostructures probably involving dynamic self-assembly of spherical micelles at the unstable interface of microemulsion droplets.[64,110] Due to the intrinsic dynamic nature of a microemulsion droplet, several common features for the synthesis of DMSNs were observed: (1) the mesostructure and morphology can be precisely tailored with the variation of the volume ratio of water to oil; (2) the successful fabrication of DMSNs is very sensitive to the stirring rate of reaction media, which significantly affects the stability of microemulsion droplets; and (3) the obtained DMSNs generally exhibit bi-modal size distributions. However, several disadvantages of MET methods should be noted: (1) reproducible synthesis is not readily accessible due to the sensitivity of reaction parameters to the stability of microemulsion nanodroplets; (2) the large quantity of organic oils used is not good for the environment and is expensive, which limits the large scale synthesis of DMSNs.

Open Access Article. Published on 16 April 2020. Downloaded on 2/9/2026 9:27:09 AM.
This article is licensed under a Creative Commons Attribution-NonCommercial 3.0 Unported Licence.

2.2. Organosilane assisted co-condensation (OAC) method

Silanes are silicon chemicals that possess a hydrolytic sensitive center that can react with an inorganic substrate to form stable covalent bonds and undergo an organic substitution that alters the physical interactions of treated substrates. Depending on the structure of silanes, there are two types of silane coupling agents. Most of the widely used organosilanes have one organic substituent and three hydrolysable substituents (also called monopodal silanes). The general formula for this type of silane coupling agent is: R–$(CH_2)_n$–Si–X_3. X is a hydrolysable group, typically alkoxy, acyloxy, halogen or amine. The R group is a non-hydrolyzable organic radical that may have the function of imparting desired characteristics. The other type of silane is bridged silsesquioxanes with the formula of X_3Si–R–SiX_3 (dipodal silanes). The most common organic groups introduced in the dipodal silanes are disulfides, diamines, benzene, *etc.* In fact, the bridged silsesquioxane precursors are first used to synthesize periodic mesoporous organosilicas (PMOs), and using the same synthetic principle of PMOs, the synthesis of DMSNs would be possible.[13] In order to distinguish DMSNs prepared by the MET method, the obtained MSNs were named dendritic mesoporous organosilica nanospheres (DMOSNs).

Freire's group first reported the preparation of DMOSNs by the one-pot soft-templating co-condensation strategy with hydrophobic tridecafluorooctyltriethoxysilane (F13) as the organosilane and TEOS as the silicon source (Fig. 7a–c). The authors demonstrated that the morphology and mesostructure of DMOSNs were strongly dependent on the amount of organosilane F13 used. Indeed, the preparation of DMSNs is an unexpected result, whereas the objective was to develop a methodology to generate superhydrophobic and superoleophobic fabrics functionalized with F13-MSNs. A more sophisticated OAC approach was developed by Paula and his coworkers using dual organosilanes of phenyltriethoxysilane (PTES) and 3-(trihydroxysilyl)propylmethyl-phosphonate (THSPMP) as silicon sources;[92] by simply adjusting the molar ratio of organosilane to TEOS, well-defined and monodispersed dendritic mesoporous organosilica nanospheres (DMOSNs) with radial ultra-large porous structures and a particle size of ~60 nm could be readily obtained (Fig. 7d–f).

Recently, following the similar synthetic principle, Shi and his coworkers reported the facile synthesis of DMOSNs with bis [3-(triethoxysilyl)propyl] tetrasulfide (BTES) as the organosilane by the one-pot co-condensation strategy.[93] They discovered that the hydrophobic $CH_2CH_2CH_2$–S–S–S–S–$CH_2CH_2CH_2$ fragment in BTES was preferentially located at the interface of CTAC micelles, which cooperatively directed the self-assembly of micelles triggered by adsorption of anionic silicate species (Fig. 8). Very interestingly, the obtained DMOSNs also exhibited bi-modal pore size distributions (Fig. 8g), similar to those of DMSNs synthesized by the MET mechanism. Very recently, our experimental results also evidenced that the use of more hydrophobic organosilanes, such as 1,2-bis(triethoxysilyl) ethane (BTSE) and 1,4-bis(triethoxysilyl)-benzene (BTSB), promoted the formation of DMOSNs,[111] suggesting the unique role of hydrophobic organosilanes in tuning the synthesis of DMOSNs. Most recently, Yang and his coworkers demonstrated that the reaction time determines the compositional and structural properties of DMOSNs: for the aqueous phase route, a prolonged reaction time is beneficial for improving the organosilica content, but leads to the loss of the porous structure; in contrast, for the water/oil biphasic route, prolonging the reaction time causes a reduction of the organic content in the products, but facilitates the formation of a well-defined dendritic mesoporous structure.[103]

In summary, the only difference in the single phase OAC method is the use of hydrophobic organosilanes to substitute the oil phase of the water–oil binary system of the MET methodology, which indicates that the organosilane involves the self-

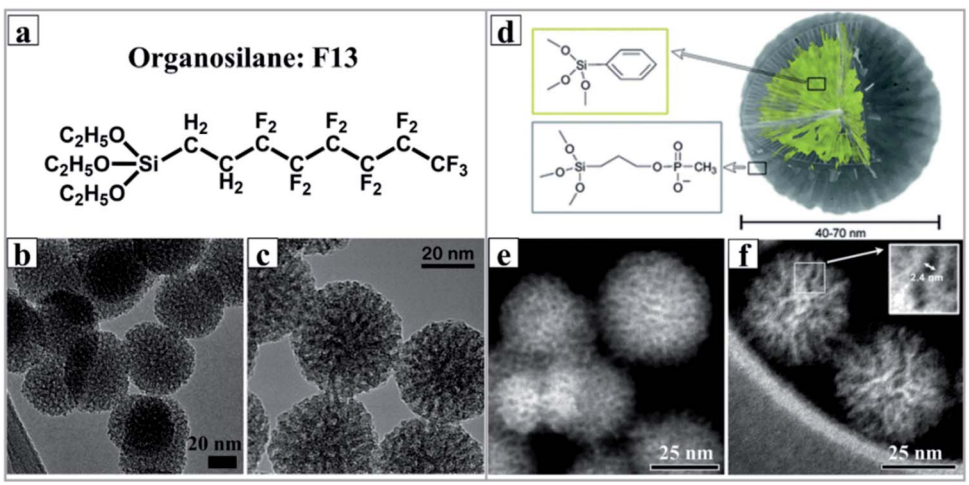

Fig. 7 (a) The chemical structure of organosilane F13 and the TEM image of mesoporous silica nanoparticles synthesized with a molar ratio of F13/TEOS of 1 : 10 (b) and 1 : 5 (c).[91] Reproduced with permission from ref. 91. Copyright 2011 American Chemical Society. (d) A cross section of the conceptual model of a multifunctionalized SiO_2 nanoparticle prepared by Paula,[92] and the STEM micrographs of unfunctionalized (e) and phenyl-decorated SiO_2 nanoparticles (f), scale bar = 25 nm. Reproduced with permission from ref. 92. Copyright 2012 The Royal Society of Chemistry.

Open Access Article. Published on 16 April 2020. Downloaded on 2/9/2026 9:27:09 AM.
This article is licensed under a Creative Commons Attribution-NonCommercial 3.0 Unported Licence.

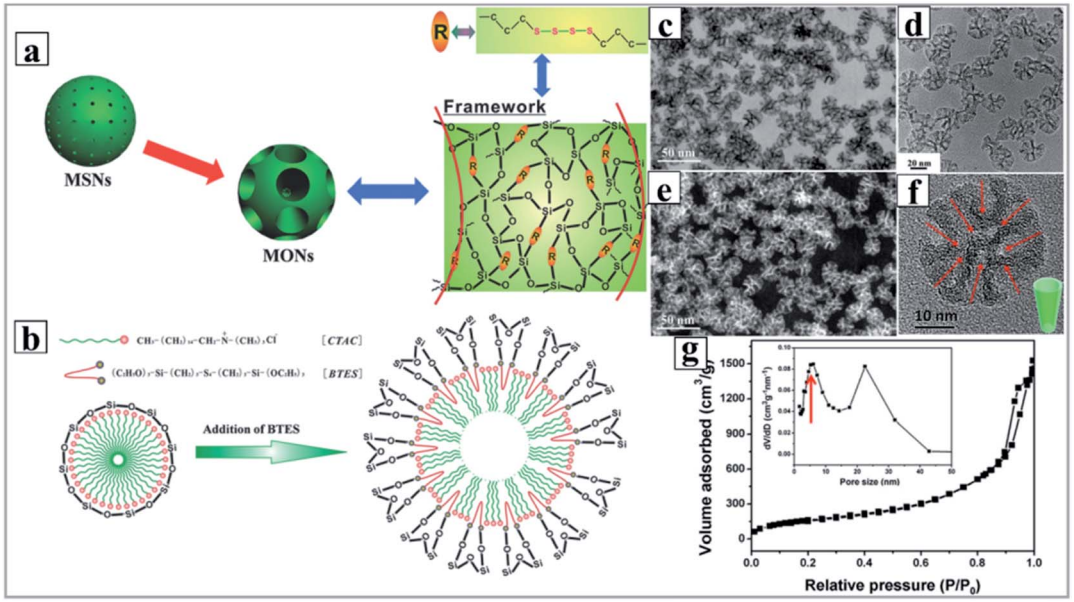

Fig. 8 (a) Schematic representation of the molecular organic–inorganic hybrid composition of thioether-bridged DMOSNs. (b) The proposed M/P-CA strategy to enlarge the micelle size of CTAC by incorporating the hydrophobic long organic chains of the as-hydrolyzed BTES into the hydrophobic part of the initially formed CTAC micelles. And corresponding TEM images (d and f) of DMOSNs at different magnifications (inset of (f): the pore shape of DMOSNs). Bright-field (c) and dark-field (e) STEM images of DMOSNs. N_2 adsorption–desorption isotherm (g) and (inset of (g)) the corresponding pore size distribution of DMOSNs.[93] Reproduced with permission from ref. 93. Copyright 2015 Wiley-VCH.

assembly of micelles and inorganic silicates. We propose that the OAC method indeed follows the same synthetic principle as that of the MET method, where unhydrolyzed or partially hydrolyzed hydrophobic organosilanes were used as the oil phase for the spontaneous formation of microemulsion nanodroplets. This conclusion was evidenced by the recent discovery of Wang and his coworkers. They demonstrated that added (3-chloropropyl)trimethoxysilane (CPTMS) played key roles in controlling the size and maintaining the metastable state of the water nanodroplets through insertion of the hydrophobic tail of the $ClCH_2$–$(CH_2)_2$–Si(–O–)$_3$ fragment and subsequently induced the formation of silica nanotubes (NBs).[112–115] Compared to the multi-step post-synthetic grafting technique,[116–118] the one-pot OAC method for the synthesis of DMSNs with customer-tailored applications is simple and reproducible. However, very rare examples were reported for the synthesis of DMSNs by this method due to the limitation of commercially available organosilanes. Additionally, the incorporation of organic functional groups into the pore wall prohibits the subsequent post-synthetic modification, thereby limiting the widespread use of this group of nanomaterials.

2.3. Spherical micelle self-aggregated assembly (SMSAA) strategy

Although the two strategies of MET and OAC are seemingly completely different, they indeed follow the same micro-emulsion template mechanism, which has been evidenced by solid experimental data. But at present, considering several pivotal aspects of synthesis with environmental concerns, involving a large quantity of toxic and/or highly inflammable organic solvents and the deliberate choice of silane coupling agents, the development of facile and green synthetic methods is particularly desired. In 2011, using the surfactant cetyltrimethylammonium tosylate (CTATos) as a new template at ultralow concentration, we reported for the first time the eco-efficient synthesis of a family of ordered mesoporous silica with varied topology, including hexagonal, cubic and rectangular phases.[119,120] The key to this method is the deliberate use of the surfactant CTATos with the strong affinity of tosylate (Tos^-) as a counter anion. Because Tos^- lies to the end of the typical anion lyotropic series, the critical micelle concentration (CMC) of the cationic surfactant is significantly reduced, and adsorption of Tos^- onto the surface of cationic micelles by regulating the interfacial charge density leads to the diversity of mesostructures. Subsequently, inspired by Bein's pioneering research on the preparation of MSNs using triethanolamine ($TEAH_3$) as the quenching molecules for the growth of NPs,[23–25] $TEAH_3$ with dual roles of a quenching agent and alkali source was introduced in our reaction system with CTATos as the surfactant template. As expected, the conventional MSNs with worm-like morphology were obtained.[118] However, the large quantity of small organic amines (SOAs) used is not environmentally friendly, since the subsequent recovery and removal of these SOAs normally requires complicated chemical processes, for example, the high-temperature combustion that destroys these high-cost components produces hazardous NO_x as well as greenhouse gases (CO_2).[121]

According to the basic principle of sol–gel chemistry, hydrolysis of the Si–OR bond in TEOS could be catalyzed by both acids and bases; thus in theory, for the classic $\{S^+I^-\}$ synthetic route under alkaline conditions (wherein S^+ means

Open Access Article. Published on 16 April 2020. Downloaded on 2/9/2026 9:27:09 AM.
This article is licensed under a Creative Commons Attribution-NonCommercial 3.0 Unported Licence.

the cationic surfactant with positive charges and I^- denotes the silicate species with negative charges), the use of just a trace amount of base will initiate the hydrolysis of TEOS, and a neutral pH value favors maximum condensation. Obviously, the higher the pH value, the stronger the electrostatic interactions between S^+ and I^-, which accelerates the assembly between the surfactant and silica. Thus, in conventional synthesis of MSNs, the reaction was generally performed at a high pH value (generally above pH = 11). Fully taking account of the kinetics of hydrolysis and condensation of TEOS, by precise pH adjustments of the reaction mixture, we achieved for the first time massive synthesis of DMSNs with dendritic pore channels on the kilogram (kg) scale using SOAs of catalytic quantity as the alkali source (extremely low molar ratio of SOAs/TEOS less than 0.026),[95] and by various adjustments of reaction parameters, including the pH of the reaction mixture, the characteristics of the surfactants or copolymers used, and the concentrations and the sources of silica, diverse MSNs with a controlled particle size and varied morphologies such as raspberry-like (RB) and worm-like channel morphologies, were also obtained (Fig. 9).[122]

Compared to the reported MAT and OAC strategies, our method is very simple, containing only TEOS/CTATos/$TEAH_3$/water ternary components, and the reaction takes place under very mild conditions (at 80 °C for 2 h) with a low water/silica ratio of 80 at an extremely low surfactant concentration (CTATos/TEOS = 0.06), and most importantly form the viewpoint of green synthesis, it is free of any exotic organic solvent,[95] which is very similar to the synthesis of standard silica NPs by the classic Stöber method.[123] This may tell us why our synthetic strategies have been widely adapted and expanded in a very short time.[100] In order to take great advantage of this review paper for propagation, the optimal synthetic details for DMSNs are described as follows: 1458.0 g of tetraethylorthosilicate (TEOS), 192.0 g of cetyltrimethyl-ammonium (CTA^+) tosylate, and 34.7 g of $TEAH_3$ were dissolved in 10 L of water. The final molar ratio of the mother liquor was $1.0SiO_2$-: 0.06CTATos : $0.026TEAH_3$: $80H_2O$. The reaction was carried out at 80 °C for 2 hours. The final pH was *ca.* 7. After filtration and drying at 100 °C for 2 hours, 460 g of the final product was collected (93% yield for SiO_2 and the surfactant). The obtained DMSNs exhibit typical dendritic morphology, and very interestingly, the characterization by N_2 adsorption shows bimodal pore size distributions at ~2.6 nm and ~15 nm, respectively, to a certain degree, implying the similarity to the mechanism with MET and OAC methods.

A three-step formation mechanism based on self-assembly and ion competition onto the micelle surface is proposed as follows: (I) the formation of partly silicated single micelles, which was also discovered by Wiesner and Zhao,[124,125] (II) block formation using these micelles as the primary building unit, and (III) block aggregation into dendritic morphology (Fig. 9a). At the single micelle level, the curvature of the organic–inorganic electrical interface was affected by the counterions (X^-) remaining in the material. This can be described as $\{(1 + n)S^+, nX^-, I^-\}$. The pivotal role of the counterions in forming the pore network is rationalized by the much lower affinity of Br^- than Tos^- for the electrical palisade of the CTA^+ micelles. Tos^- competes more strongly against the adsorption of silicate oligomers on the micelles than Br^-, which is more favored at a low pH value. Indeed, the silanolate density (I^-) is too small to displace Tos^- anions efficiently. We named this phenomenon "weak templating" interactions. In contrast, high SOA concentrations (pH ≈ 10) and high silanolate densities result in stronger templating conditions, yielding MSNs with a more organized 1D worm-like array of the pore channels, like MCM-41 and SBA-15 silicas.

Because self-assembly takes place between polymerized silicate oligomers and individual or single surfactant micelles, we named this synthetic strategy the spherical micelle self-

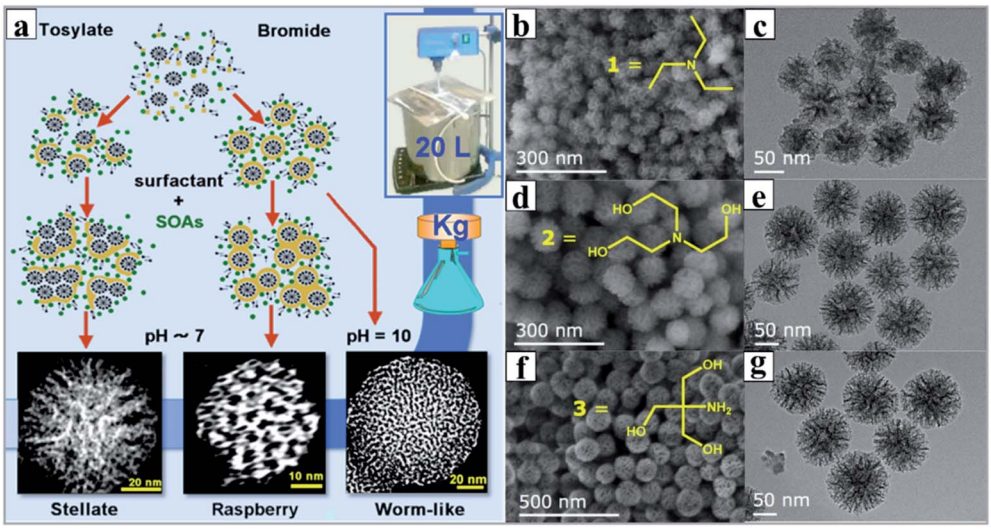

Fig. 9 (a) Scale-up synthesis with tunable mesostructures *via* the mono-micelle templating self-assembly strategy, and SEM (b, d and f) and TEM (c, e and g) images of samples synthesized with different small organic amines (SOAs) of triethyleneamine (b and c), triethanolamine (d and e), and 2-amino-2-(hydroxymethyl) propane-1,3-diol (f and g).[95] Reproduced with permission from ref. 95. Copyright 2013 American Chemical Society.

 This journal is © The Royal Society of Chemistry 2020

Open Access Article. Published on 16 April 2020. Downloaded on 2/9/2026 9:27:09 AM.
This article is licensed under a Creative Commons Attribution-NonCommercial 3.0 Unported Licence.

aggregated assembly (SMSAA) mechanism, highlighting the key role of the surfactant counterions and pH value in tuning the morphology of MSNs using single spherical micelles as the primary building unit. The imperfect-centered dendritic morphology indicates that the nucleation and growth processes occur *via* a block-by-block aggregation, wherein the block as a secondary building unit is composed of primary building units of single micelles. A similar experimental phenomenon was observed in the synthesis of silicate-1 zeolite.[126] The mesochannel morphology is controlled by the template counterion and the SOA concentration, which were determined by weaker or tighter templating interactions between silicate species and single micelles.

To further prove the competing adsorption of counter anions on the positive micelles to negative silicate species, anionic surfactants, such as sodium dodecyl benzene sulfonate (SDBS), sodium dodecyl sulfate (SDS), sodium laurate (SL) and sodium stearate (SS), were introduced to synthesize DMSNs in the presence of conventional cationic CTABr surfactants (Fig. 11).[122] In the current cationic-anionic surfactant dual-templating strategy, the anionic surfactant has a much higher affinity than the Tos^- anion for the electrical palisade of the CTA^+ micelles due to the very strong hydrophobic forces between the long carbon chains. The presence of the anionic surfactant in the mixed surfactant micelles strongly counteracts the competitive adsorption of silicate oligomers (I^-) on the mixed CTA^+ micelles due to the electrostatic repulsion relative to the single cationic CTA^+ micelles. Thus, following the same SMSAA mechanism mentioned above, DMSNs were finally obtained. Moreover, by finely tuning the molar ratio of dual-templates, MSNs with varied morphologies, including silkworm cocoon-like (SW-MSNs) and mono-lamellar vesicle (V-MSNs), were also synthesized (Fig. 10a, bottom). Again, the common feature of DMSNs with dual size pore distributions of ~4.0 nm and ~21 nm was also observed (Fig. 10a). With detailed treatment of the TEM image of individual DMSN nanospheres (Fig. 10b), the blocks composed of single micelles with a size of ~4.0 nm could be distinguished, like 'the single micelle filling in the dendritic channels', which clearly reveals the origin of the smaller pore size distribution for all the DMSNs obtained by N_2 adsorption (Fig. 10c).

More investigations following this concept showed that not only other anionic surfactants and small organic anions (such as fluorocarbon anions[99–102] and sodium salicylate[97,98,127]), but also nonionic surfactants could play the same role in the synthesis of DMSNs.[128] Among these reports, Yu and his coworkers performed much more elegant research, not only on the synthesis and applications of DMSNs (especially in the biomedical field), but also on a completely new and in-depth understanding of the dynamic structural changes.[71,100] A new micelle filling mechanism was proposed in these studies to reveal the dynamic structure change from a dahlia-like morphology to a pomegranate-like morphology (Fig. 11). Based on this mechanism, the final structures of DMSNs with bimodal pore size distributions were rationally elucidated: the silica-coated micelles are heterogeneously nucleated on a preformed large dendritic pore surface due to further condensation between silanol groups, and subsequent surfactant removal results in the formation of small mesopores (nanocast by single spherical micelles in Fig. 11B2) and large dendritic pores (Fig. 11B1), and the extent of micelles filling the dendritic large

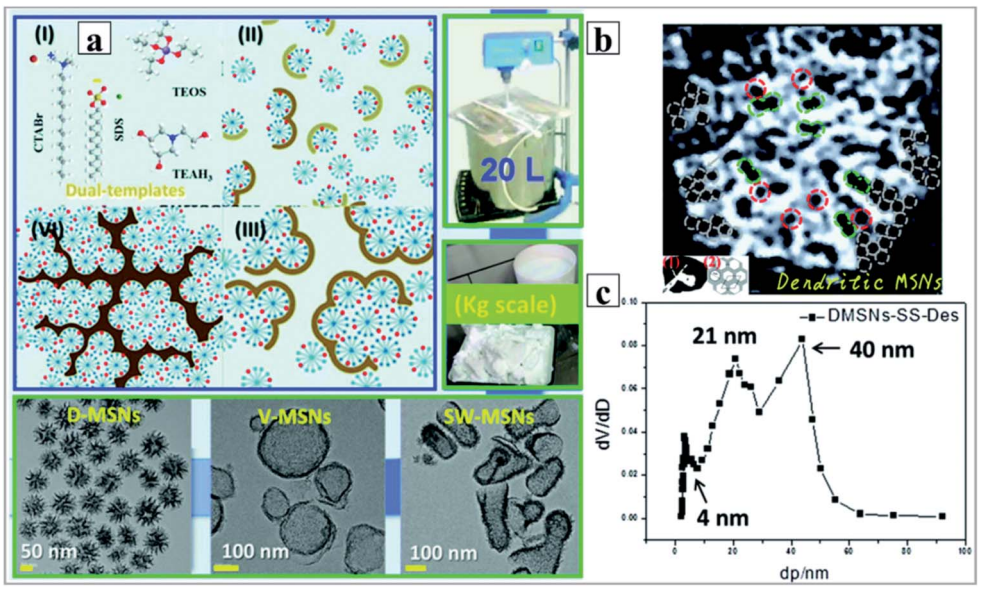

Fig. 10 (a) Dual template synergistically controlled micelle self-aggregated model to understand the formation mechanism of dendritic MSNs; (b) pore networks of the typical dendritic MSNs observed by TEM. The red, green and brown circles indicate the small, intermediate and large pores using monomicelles, bimicelles and aggregated micelles as the templates or structure building units, respectively (inset 1, pore networks of classical amorphous silica sol particles; inset 2, the hexagonal pore array of MCM-41 or SBA-15); (c) pore size distribution (PSD) of typical dendritic MSNs synthesized by using the dual-templating strategy in the presence of the anionic sodium stearate (SS) surfactant calculated by the BJH method from both desorption branches.[122] Reproduced with permission from ref. 122. Copyright 2017 The Royal Society of Chemistry.

Open Access Article. Published on 16 April 2020. Downloaded on 2/9/2026 9:27:09 AM.
This article is licensed under a Creative Commons Attribution-NonCommercial 3.0 Unported Licence.

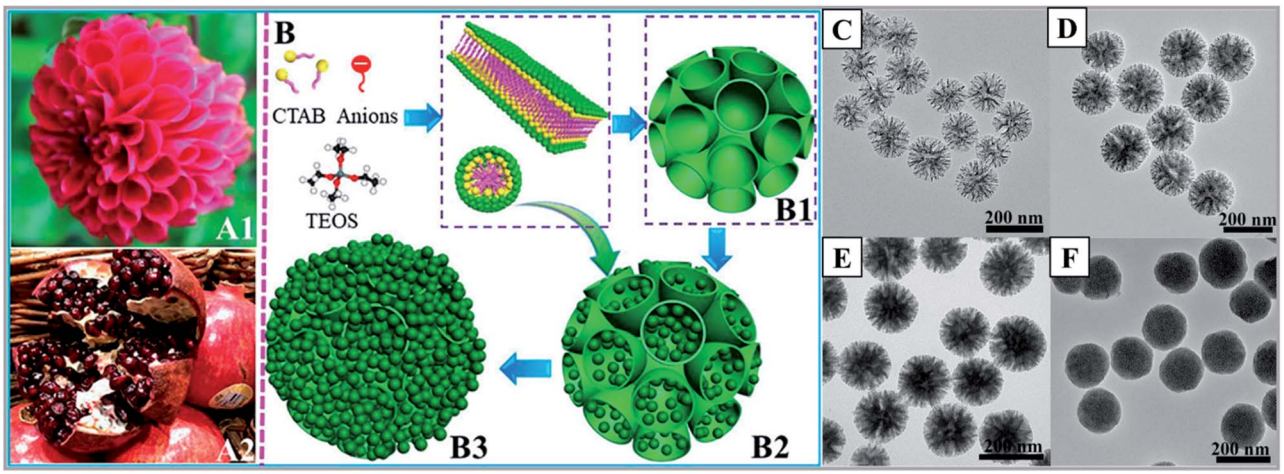

Fig. 11 (A1) A dahlia-like DMSN and (A2) a pomegranate-like MSN and (B) the kinetic micelle filling mechanism. The dahlia-like DMSNs (B1) are first assembled by an anion-assisted approach through lamellar building blocks. By gradually filling the large dendritic pores with composite micelles, we obtained a series of intermediate structures (B2) and small-pore MSNs with the dendritic pores completely filled (B3). Objects are not drawn to scale; TEM images (C–F) of MSNs at a fixed reaction temperature of 80 °C and a FC2/CTAB molar ratio of 1 at various reaction times of (C) 0.3, (D) 1, (E) 2, and (F) 5 h.[100] Reproduced with permission from ref. 100. Copyright 2018 American Chemical Society.

pores finally determines the final fractions of small mesopores in DMSNs.[100]

By combining other reported mechanisms, a universal spherical micelle self-aggregated assembly (SMSAA) mechanism was proposed to understand the formation mechanism for the synthesis of MSNs by precisely tuning the electrostatic interactions between silicate species and single micelles (Fig. 12).[128] Depending on the strength of interfacial charge shielding, three types of MSNs with varied kinetically controlled heterogeneous structures were synthesized. At a high pH value in the presence of the conventional surfactant CTABr, generally called the modified Stöber method,[34,37,123,129] traditional MCM-41 and MSNs were finally obtained due to very strong electrostatic interaction of $\{S^+I^-\}$, where the primary building unit (PBU) could be spherical micelles or rod-, or worm-like micelles (Fig. 12, route I). At a medium strength of $\{S^+I^-\}$ interactions, DMSNs with dendritic networks were synthesized in the presence of dual surfactants or the special surfactant counter anions with high hydrophobicity (Fig. 12, route II), where the partly silica coated single spherical micelles were used as the PBU, *i.e.*, the so called SMSAA mechanism. Obviously, the respective sizes of bimodal porosity of smaller mesopores and dendritic large pores and their relative fractions were determined by the strength of the $\{S^+I^-\}$ interactions. With very weak interactions in route III, for example, if the nonionic 4-nonylphenol branched ethoxylated surfactant (Tergitol NP-7) or polyoxyethylene sorbitan mono-oleat (Tween-80) was used as co-templates, DMSNs only show dendritic large pores without small mesopores (Fig. 12, route III). Although the detailed formation process of dendritic large pores is still under debate, a common consensus on the SMSAA mechanism using partly silica coated single spherical micelles as the PBU has been reached, and the fraction and accessibility of small mesopores located inside dendritic large pores is strongly dependent on the coverage of the silica coating on single spherical micelles, *i.e.*, the strength of $\{S^+I^-\}$ electrostatic interactions during the self-assembly processes.[95,100,122]

Compared with the MET and OAC methods with spontaneously formed microemulsion droplets as supertemplates, intuitively, the SMSAA methodology should follow a completely different mechanism for the synthesis of DMSNs because of the absence of the oil phase. However, a common feature of all the synthesis methods of DMSNs is neglected since the hydrophobic TEOS used as the silica source could act as the oil component to form the immiscible oil/water biphases, especially at the early stage of the reaction. Thus, now the question is whether all the DMSNs follow the same synthetic principles? Very recently, both experimental and theoretical studies evidenced that ternary solutions containing one hydrotrope (such as ethanol) and two immiscible fluids, both being soluble in the hydrotrope at any proportion, showed unexpected solubilization power and the presence of 'detergentless' micelles or microemulsions in such mixtures,[130–134] a phenomenon that is called the 'pre-Ouzo' structure effect. The spontaneous formation of fine emulsions with a remarkable stability provides a supertemplate for the synthesis of DMSNs in the early reaction stage, explaining the intermediate or dynamic nature of DMSNs with dendritic larger pores.[100,111] Recently, by just a simple premixing of three components, tetraethoxysilane–water–ethanol (TEOS–H_2O–EtOH), we reported for the first time that the MSNs were synthesized even in the absence of organic surfactant templates. The formation of mesoporosity is attributed to the leaching or dissolution and recondensation of the unreacted silicon species contained in the 'pre-Ouzo' structure, which was spontaneously preformed in the ternary TEOS–H_2O–EtOH system as a metastable microemulsion self-template.[135] Thus we concluded that, even in the absence of an organic additive (or oil phase), in the TEOS (or partially hydrolyzed TEOS)/ethanol/water ternary system, especially at a very early stage

 This journal is © The Royal Society of Chemistry 2020

Open Access Article. Published on 16 April 2020. Downloaded on 2/9/2026 9:27:09 AM.
This article is licensed under a Creative Commons Attribution-NonCommercial 3.0 Unported Licence.

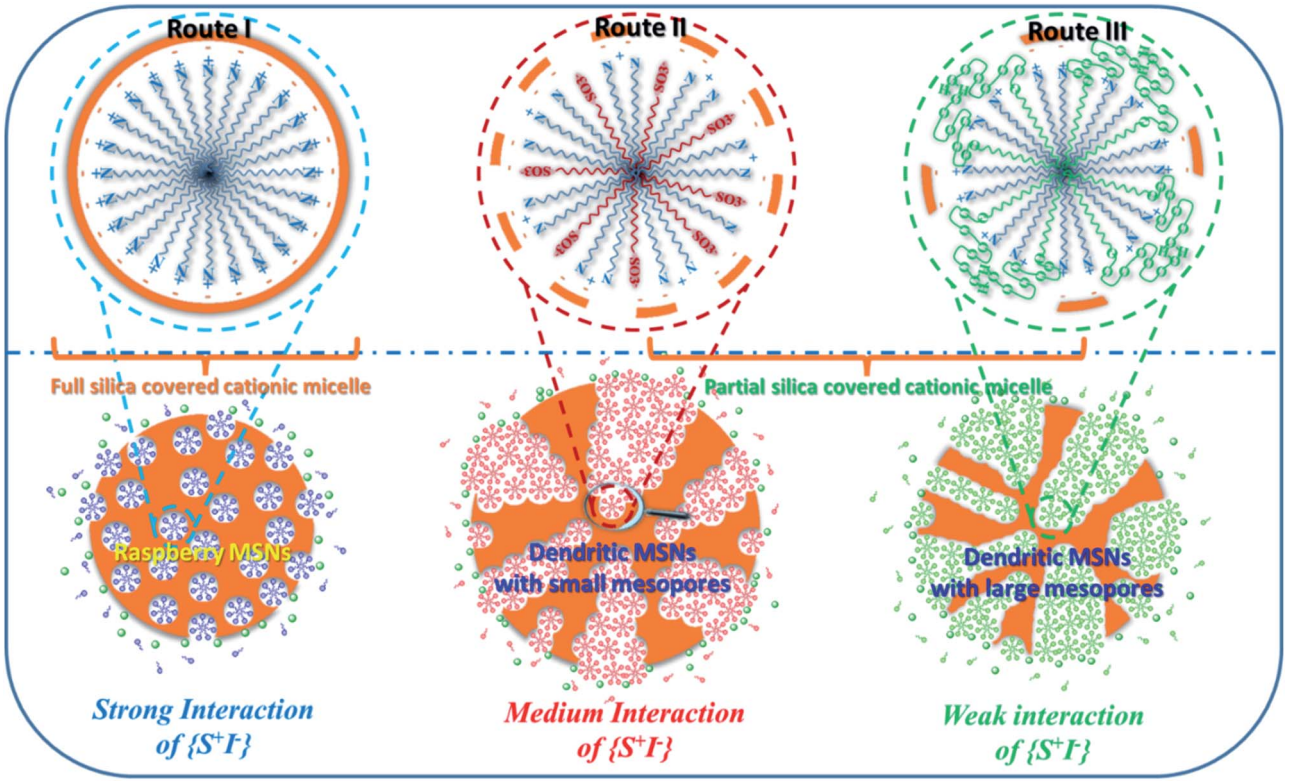

Fig. 12 Interfacial charge shielding (ICS) directs the synthesis of MSNs with varied mesostructures by precisely controlling the interactions between the cationic surfactant micelle (S^+) and negative inorganic silicate species (I^-): route I, solo template method using a single CTA^+ surfactant for the synthesis of MSNs and MCM-41 silica at a high pH value; route II, the cationic–anionic dual surfactant template approach for dendritic MSNs with 3.0 nm mesopores using the anionic sodium dodecyl sulphate (SDS) surfactant as the co-template; route III: the cationic–nonionic dual surfactant template strategy for dendritic MSNs with large mesopores (>5.0 nm) using nonionic NP-7 or Tween 80 as the co-template.[128] Reproduced with permission from ref. 128. Copyright 2019 The Royal Society of Chemistry.

of the reaction, the spontaneously formed microemulsion droplets by the 'pre-Ouzo' effect could act as the supertemplate to direct the formation of dendritic large pores, and with the reaction proceeding, the partly silica coated spherical micelles are deposited onto the supertemplate of the microemulsion droplets, consequently leading to the formation of DMSNs with bimodal pore size distributions. In brief, DMSNs are indeed a product or the result of a two-level template collaborative self-assembly process of microemulsion droplets and micelle templates. However, obtaining more details on the influence of the 'pre-Ouzo' effect on the mesostructures of DMSNs needs more investigations in the near future. It is important to note that even though the 'pre-Ouzo' effect was intensively studied in surfactant chemistry, the application of the pre-Ouzo effect in the synthesis and mechanistic understanding of the mesoporous silica and even Stöber silica NPs was seldom investigated, and it should develop into one of the most cutting-edge research directions in nanomaterials science. To sum up, all three types of methods for the synthesis of DMSNs, including MET, OAC and SMSAA protocols, follow the same synthetic principle, revealing the unique structural features of bimodal pore size distributions and dendritic pore networks in an individual nanosphere.

3. A new generation of nanoreactors for the heterogeneous catalysis and the fabrication of PL materials

Even though diverse synthetic strategies were reported to synthesize DMSNs with varied pore sizes and morphologies, they all exhibit the identical and unique structural feature of bimodal pore size distributions, *i.e.*, the coexistence of small spherical mesopores and large dendritic pores, and their pore sizes and the fractions could be easily adjusted by precisely changing the reaction parameters. Most importantly and very fortunately, these small spherical mesopores nanocast by partly silica coated micelles are open and diffusion-accessible after the removal of the surfactant *via* high-temperature calcination or acid-extraction. This is also the reason why, in some cases, DMSNs are called three dimensional (3D) nanostructured mesoporous silica. One can imagine the dendritic channel of DMSNs as a V-shaped container filled with open hollow spheres by hard sphere close-packing. It is important to note that the published review papers mainly focused on the discussion of the applications of DMSNs in drug delivery and biomedicine by taking full advantage of the the size effect of nano-scale particles.[55–58,136,137] In this review, benefiting from the unique

Open Access Article. Published on 16 April 2020. Downloaded on 2/9/2026 9:27:09 AM.
This article is licensed under a Creative Commons Attribution-NonCommercial 3.0 Unported Licence.

structural nanoconfinement of small spherical mesopores in the dendritic networks, we highlight their applications in nanocatalysis and optical materials.

3.1. Unique nanoconfinement effect for heterogeneous catalysis

By virtue of their native structural advantage, DMSNs are extensively used as a catalytic support for various chemical reactions[111,138–151] and can be directly applied for efficient catalysis through introducing other active metal elements into the structure[77,122,128,152,153] or surface modification.[154–158] While the catalytic performance actually depends on many factors (such as the quantity, properties, micro-environment of the active site, *etc.*) and cannot be absolutely attributed to the advantage of the structure, it is still an ideal platform for the design of metal nanocluster (NC) based heterogeneous catalysts with high performance, because of the bimodal pore size distributions of DMSNs, especially the small open spherical mesopores which provide an ideal nanoreactor for the encapsulation of metal NCs of a size less than 3.0 nm. Even though, by both bottom-up and top-down synthetic strategies using protective molecules as templates, metal NCs with precise atom numbers could be easily prepared, the protective ligands on the NC core greatly limit the contact of the reaction substrate with the catalytically active sites and reduce the chemical reactivity of the catalyst.[159] Here, as a typical example, using hierarchical DMSNs as a unique confinement matrix wherein open spherical mesopores with a micelle size *ca.* 4.0 nm nested in the dendritic channels (Fig. 13a, inset), an Au/Ag bimetallic catalyst is fabricated by a multi-step *in situ* nanocrystal seeding induced-growth (SIG) strategy, which endows the alloy with an ultra-small size (~3 nm) and high dispersity (Fig. 13). The obtained Au/Ag bimetallic catalysts show an exceptional superior photocatalytic activity for the reduction of 4-nitrophenol (4-NP), outperforming most reported noble metal nanoparticle catalysts. The unusual catalytic activity originates from the high dispersity of metal NPs and the photo-irradiation enhanced electron transfer (PIEET) ability at the bimetallic nanoparticle interface due to the unique confinement effect of dendritic mesoporous silica nanoparticles (DMSNs) wherein open spherical mesopores with a micelle size (*ca.* 3.0 nm) nested in the dendritic channels.

In another example, Peng and his coworkers conceptually developed a "catalysts in coronas" strategy to prepare highly active nickel (Ni) nanoparticle (NP) catalysts for the methane dry reforming reaction, using DMSNs as a support for Ni NPs (Fig. 14).[160] The obtained Ni NP based catalyst exhibited an excellent catalytic performance with a long life time (145 h) and high conversion of 76% at 700 °C, which is close to its equilibrium conversion. The authors concluded that sintering of Ni NPs and coking resistance originated from the surface spatial confinement effect where the three-dimensional dendritic layers in the corona posed a steric barrier against migration and aggregation of Ni NPs. These findings shed new light on the design of other metal- or metal oxide-supported catalysts especially for high-temperature heterogeneous catalytic reactions, such as the gas-phase oxidation and the water gas shift reaction (WGSR).

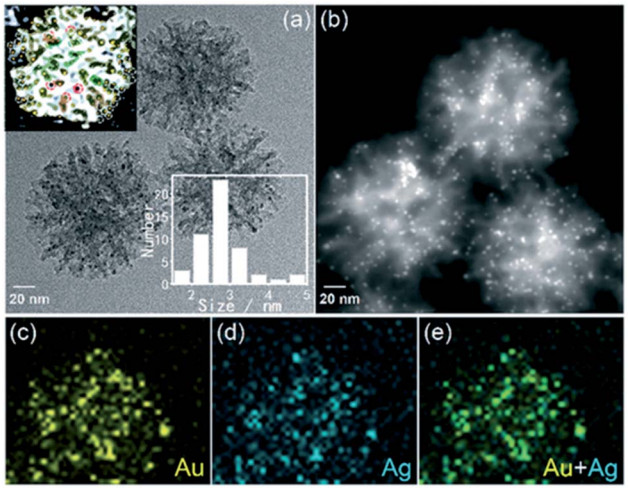

Fig. 13 Bright-field TEM (a) and high-resolution HAADF-STEM (b) images of 1% Ag_2O/1% Au-DMSNs. Corresponding STEM EDX mapping images of Au/Ag_2O: (c) Au (yellow), (d) Ag (blue) and (e) Au/Ag merged (green), respectively. The inset in (a) shows that DMSNs have small, ill-ordered spherical pores (~3 nm) nested in the dendritic channel networks.[151] Reproduced with permission from ref. 151. Copyright 2019 The Royal Society of Chemistry.

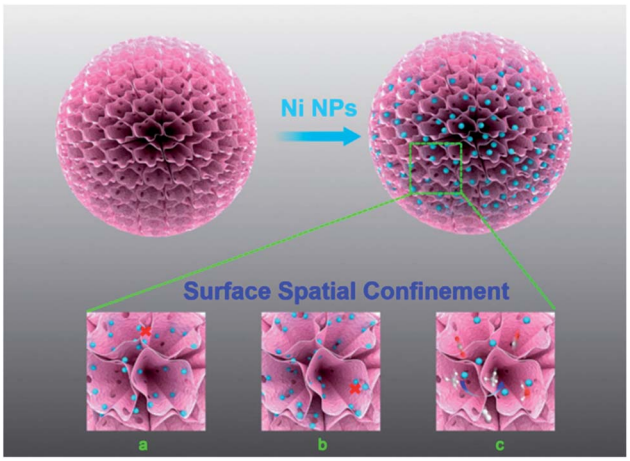

Fig. 14 Illustration of the surface spatial confinement strategy (red spheres: Ni NPs). (a) Ni NPs between the layers are prevented from migrating; (b) Ni NPs between the mesopores are prevented from migrating; (c) reactants can be transferred freely between the mesopores.[160] Reproduced with permission from ref. 160. Copyright 2013 American Chemical Society.

3.2. Fabrication of photoluminescent (PL) materials by post-functionalization of non-conjugate organic groups or by the immobilization of perovskite quantum dots (QDs) using DMSNs as silica matrix

Due to the interesting photoluminescence (PL) properties, zero-, one- and two-dimensional quantum nanomaterials attract much more interest, including noble metal

 This journal is © The Royal Society of Chemistry 2020

Open Access Article. Published on 16 April 2020. Downloaded on 2/9/2026 9:27:09 AM.
This article is licensed under a Creative Commons Attribution-NonCommercial 3.0 Unported Licence.

nanoclusters (NCs), semiconductor quantum nanostructures (black phosphorus nanosheets and transition metal dichalcogenides as typical examples), and carbon (or graphene) quantum dots (QDs).[159,161–165] However, the green and reproducible synthesis of NC based QDs with tunable colors is challenging. In addition, even though the nanocluster-centered free-electron model based on the quantum confinement mechanism has been well accepted, the elucidation and origin of optoelectronic properties have been diverse and contradictory over the past decade.[166–173] More and more experimental evidence has proved that the distribution of surface protecting ligands (or clustering of the surface) on the metal core played a paramount role in tuning the optoelectronic properties of noble metal NCs.[169,170,174]

Inspired by the fundamental understanding of the origin of metal NC PL dominated by the p band intermediate state (PBIS) model, recently, using DMSNs as the support, we demonstrated that the self-assembly of organic functional groups in spherical mesopores using the post-grafting technique produced a stable and bright AIE-type luminogen as an emitter for PL emission free of any metals (Fig. 15a and b).[175] It is important to note that the functional groups of the selectively used organosilanes contain heteroatoms with unpaired lone electrons, such as oxygen (O), nitrogen (N), and sulfur (S), used as protecting ligand molecules for the synthesis of metal NCs. The characterization of optical absorption and PL emission spectra showed that the luminescent mesoporous silica nanoparticles functionalized with nonluminescent organosilanes exhibit the same spectroscopic properties as metal NCs and that their PL properties strongly depend on the nature of organic functional groups: the amino-functionalized DMSNs showed a striking blue-light fluorescence emission at *ca.* 430 nm, and their excitation and emission spectra completely matched, implying an AIE luminogen emission mechanism (Fig. 15c), while the succinic functionalized DMSNs exhibited a remarkable red-color emission at *ca.* 615 nm (Fig. 15d).

Note that both single amino and succinic functional groups are nonluminescent. It is reasonable that, in the confined nanospace of DMSNs, the self-assembly of the amino and carboxylate groups, by through space electronic interactions, namely, overlapping of the p orbital of lone pair (*n*) electrons among amino and carbonyl groups, extends the conjugation;

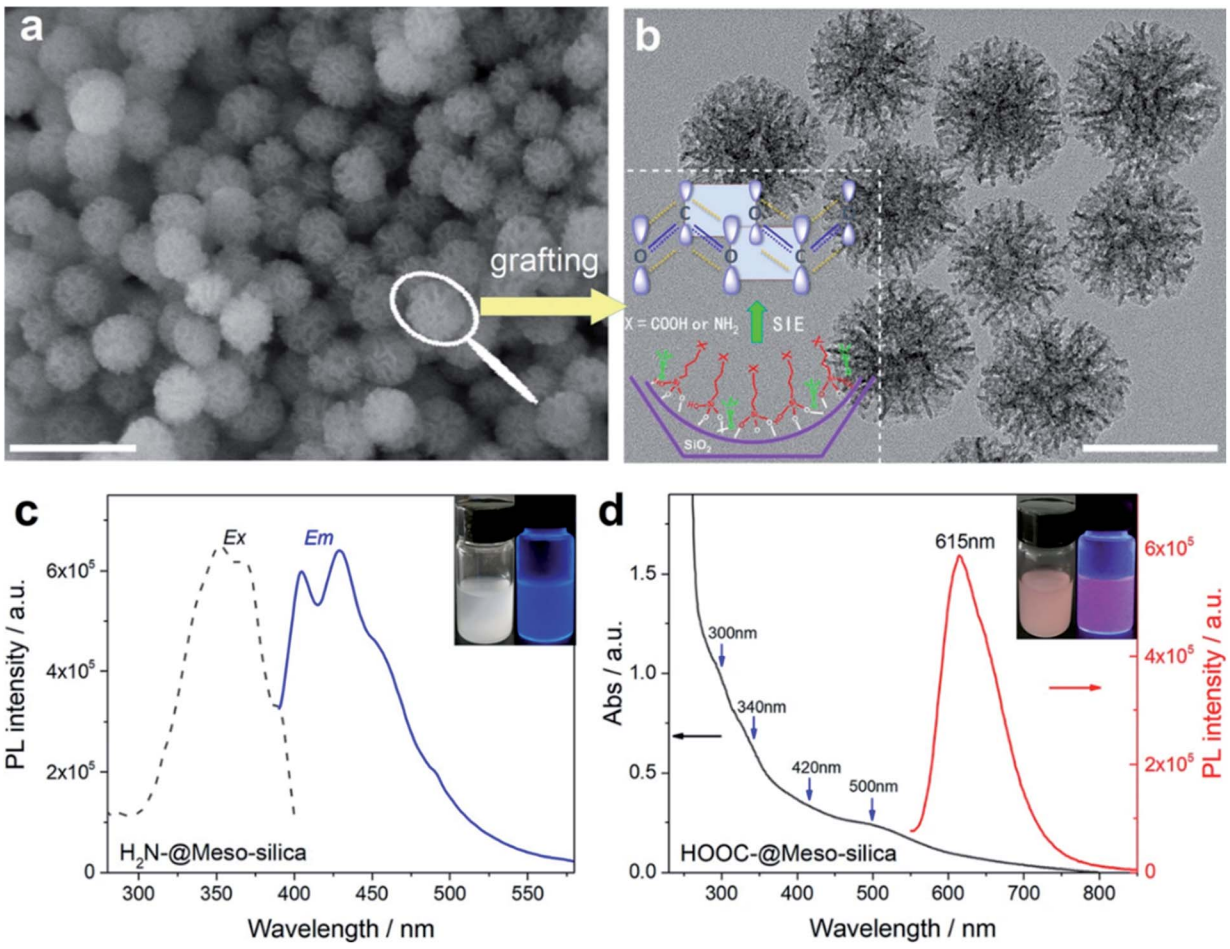

Fig. 15 Ligand assembly in the MSNs free of metals and their tunable luminescence properties. Scanning electron microscopy (SEM) (a) and TEM (b) images of the as-synthesized fluorescent mesoporous silica nanoparticles. The inset shows the assembly of amino- and carbonyl-groups in the confined nanopores (the scale bar in a and b is 200 and 100 nm, respectively). (c) Excitation and emission spectra of aminopropyl-functionalized MSNs. (d) Absorption and emission spectra of propylsuccinic-functionalized MSNs.[175]

Open Access Article. Published on 16 April 2020. Downloaded on 2/9/2026 9:27:09 AM.
This article is licensed under a Creative Commons Attribution-NonCommercial 3.0 Unported Licence.

thus, the corresponding intense and multiple absorption bands in the range of 300–500 nm are observed with subsequent PL emissions (Fig. 15c and d). So far, to the best of our knowledge, this is the first example that simple organic functional-group-modified DMSNs can emit a very strong PL by the self-assembly of targeted molecules with electron-rich heteroatoms in the confined nanopores.[175] The successful synthesis of PL DMSNs, in turn, clearly demonstrates for the first time that the bright PL of few-atom metal nanoclusters originates from the self-assembly of surface ligands, providing direct evidence of the effectiveness and rationality of the p band dominant ligand-centered model for the elucidation of the photochemistry and photophysics of low dimensional quantum nanomaterials relative to the conventional metal-centered free-electron model.[159]

DMSNs are also an ideal matrix for the synthesis of $CsPbBr_3$ perovskite QDs. Taking full advantage of the unique open 3D porous architecture of dendritic mesoporous silica nanospheres (DMSNs) with cage-like spherical nanopores, highly dispersed and pure cubic $CsPbX_3$ QDs were successfully immobilized onto the mesoporous networks by a combined chemical anchoring and spatial isolation strategy.[165] The fabricated $CsPbX_3$@HA-DMSNs exhibit excellent luminescence properties (tunable emission color and high quantum yield (the QY reached a maximum of 55%)) and enhanced stability (especially for the water resistance capacity) (Fig. 16). The photoluminescence (PL) was sustained without any distinct change after 100 d of storage under ambient conditions; even 90% PL intensity was maintained after continuous UV irradiation for 45 h and no obvious PL reduction was observed when soaked in water for 7 h. Therefore, DMSNs with unique mesostructures provide an alternative candidate for light-emitting materials for display devices as a stable support.

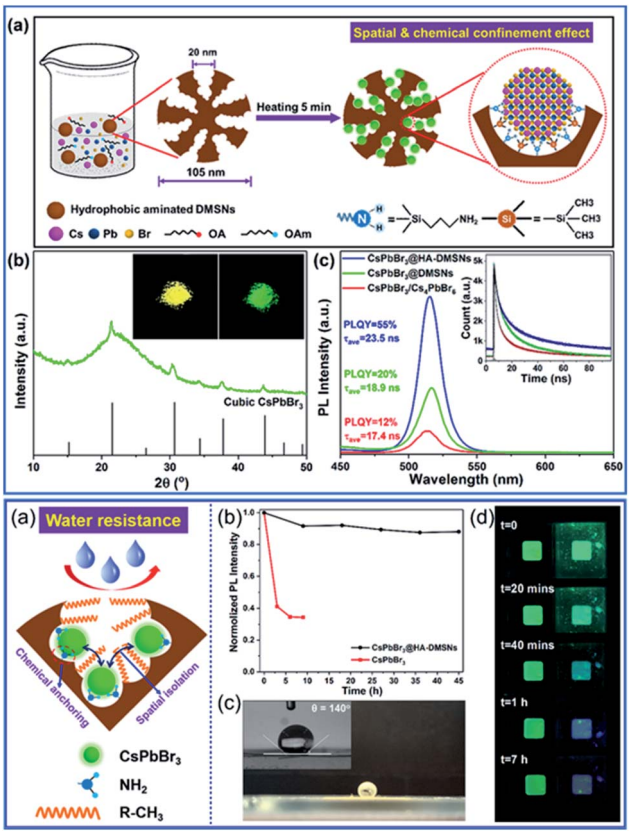

Fig. 16 Spatially and chemically confined ultra-small $CsPbBr_3$ perovskite QDs in dendritic mesoporous silica nanospheres with enhanced stability for the fabrication of LEDs.[165] Reproduced with permission from ref. 165. Copyright 2020 Elsevier Ltd.

4. Summary and concluding remarks

Obviously, in surfactant-silica assembly, the complex thermodynamic and kinetic processes of sol–gel chemistry, as well as the adjustment of a large number of reaction parameters (such as the silica source, the surfactant type, the organic additives, the base source, the reaction temperature, the water content, the pH value of the reaction solution, *etc.*), cover up the real nature of DMSN formation, and different synthetic principles were proposed to understand their formation mechanism, which in turn greatly interfere with the accurate analysis of the real structures of DMSNs. By carefully analyzing the similarities and differences of each preparation approach, as well as the structural characteristics of the synthesized DMSNs, we draw the conclusion that all the synthetic strategies for DMSNs follow the same dynamic self-assembly mechanism with a synergetic dual-template role for microemulsion nanodroplets and surfactant micelles, which reveals the common structural characteristics of DMSNs with bimodal pore size distributions. Consequently, the questions posed in the abstract could be easily understood, which will guide the more rational synthesis of DMSNs toward customer-tailored applications. We believe that this elegant synthetic strategy could be easily expanded for the synthesis of other hierarchical nanomaterials with tunable morphologies and varied chemical components, such as carbon, transition metals or noble metal crystals and even microporous zeolites.

DMSNs have emerged as ideal model nanoreactors for studying heterogeneous catalysis and nanoscale surface chemistry due to their unique confined dimensions. Here, using DMSNs as a model platform, we reveal the electronic mechanisms of how the size effect and surface ligand assembly modify their catalytic activity and PL properties, respectively. In addition, we first showed that DMSNs are also an ideal matrix for the trapping of $CsPbBr_3$ perovskite QDs, which exhibited excellent PL properties with high stability. We confirmed that, in a confined nanospace, surface chemistry is affected by the particle size, and surface modification and surface ligand states can dominate the physical and chemical performances of nanomaterials. DMSNs could act as a new generation of nanoreactors to generally explore the electronic mechanisms of size dependent catalysis, ligand-induced surface effects on tuning of the electronic structures, optical properties, and device performance of nanomaterials.

Conflicts of interest

There are no conflicts to declare.

This journal is © The Royal Society of Chemistry 2020

Open Access Article. Published on 16 April 2020. Downloaded on 2/9/2026 9:27:09 AM.
This article is licensed under a Creative Commons Attribution-NonCommercial 3.0 Unported Licence.

Acknowledgements

This work was supported by the NSFC (21872053 and 21573074), the Science and Technology Commission of Shanghai Municipality (19520711400), the CAS Key Laboratory of Low-Coal Conversion Science & Engineering (KLLCCSE-201702) and the JORISS Program, Postdoctoral Science Foundation of China (2018M640360). K. Z. thanks ENS de Lyon for a temporary position as an invited professor in France. This paper is dedicated to Prof. Ming-Yuan HE on the occasion of his 80th birthday. We also acknowledge the long-term research cooperation on this topic with Prof. Laurent Bonneviot and Prof. Bélen Albela at ENS-Lyon in France and Prof. Peng Wu at ECNU in China since 2004.

Notes and references

1 J. S. Beck, J. C. Vartuli, W. J. Roth, M. E. Leonowicz, C. T. Kresge, K. D. Schmitt, C. T.-W. Chu, D. H. Olson, E. W. Sheppard, S. B. McCullen, J. B. Higgins and J. L. Schlenker, *J. Am. Chem. Soc.*, 1992, **114**, 10834–10843.
2 D. Zhao, J. Feng, Q. Huo, N. Melosh, G. H. Fredrickson, B. F. Chmelka and G. D. Stucky, *Science*, 1998, **279**, 548–552.
3 Y. Wan and D. Zhao, *Chem. Rev.*, 2006, **107**, 2822–2860.
4 A. Taguchi and F. Schüth, *Microporous Mesoporous Mater.*, 2005, **77**, 1–45.
5 B. G. Trewyn, I. I. Slowing, S. Giri, H. T. Chen and V. S.-Y. Lin, *Acc. Chem. Res.*, 2007, **40**, 846–853.
6 R. Ciriminna, A. Fidalgo, V. Pandarus, F. Beland, L. M. Ilharco and M. Pagliaro, *Chem. Rev.*, 2013, **113**, 6592–6620.
7 Y. Deng, J. Wei, Z. Sun and D. Zhao, *Chem. Soc. Rev.*, 2013, **42**, 4054–4070.
8 C. T. Kresge, M. E. Leonowicz, W. J. Roth, J. C. Vartuli and J. S. Beck, *Nature*, 1992, **359**, 710–712.
9 S. H. Wu, C. Y. Mou and H. P. Lin, *Chem. Soc. Rev.*, 2013, **42**, 3862–3875.
10 C. Boissiere, D. Grosso, A. Chaumonnot, L. Nicole and C. Sanchez, *Adv. Mater.*, 2011, **23**, 599–623.
11 C. Sanchez, C. Boissiere, S. Cassaignon, C. Chaneac, O. Durupthy, M. Faustini, D. Grosso, C. Laberty Robert, L. Nicole, D. Portehault, F. Ribot, L. Rozes and C. Sassoye, *Chem. Mater.*, 2013, **26**, 221–238.
12 D. P. Debecker, S. Le Bras, C. Boissiere, A. Chaumonnot and C. Sanchez, *Chem. Soc. Rev.*, 2018, **47**, 4112–4155.
13 F. Hoffmann and M. Froba, *Chem. Soc. Rev.*, 2011, **40**, 608–620.
14 H. Lin, Y. Chen and J. Shi, *Chem. Soc. Rev.*, 2018, **47**, 1938–1958.
15 V. Valtchev and L. Tosheva, *Chem. Rev.*, 2013, **113**, 6734–6760.
16 Q. Cai, Z. S. Luo, W. Q. Pang, Y. W. Fan, X. H. Chen and F. Z. Cui, *Chem. Mater.*, 2001, **13**, 258–263.
17 C. E. Fowler, D. Khushalani, B. Lebeau and S. Mann, *Adv. Mater.*, 2001, **13**, 639–952.
18 R. I. Nooney, D. Thirunavukkarasu, Y. Chen, R. Josephs and A. E. Ostafin, *Chem. Mater.*, 2002, **14**, 4721–4728.
19 C. Y. Lai, B. G. Trewyn, D. M. Jeftinija, K. Jeftinija, S. Xu, S. Jeftinija and V. S.-Y. Lin, *J. Am. Chem. Soc.*, 2003, **125**, 4451–4459.
20 I. Slowing, J. L. Vivero-Escoto, C. W. Wu and V. S.-Y. Lin, *Adv. Drug Delivery Rev.*, 2008, **60**, 1278–1288.
21 B. G. Trewyn, S. Giri, I. I. Slowing and V. S.-Y. Lin, *Chem. Commun.*, 2007, 3236–3245.
22 J. L. Vivero-Escoto, I. I. Slowing, B. G. Trewyn and V. S.-Y. Lin, *Small*, 2010, **6**, 1952–1967.
23 K. Möller, J. Kobler and T. Bein, *Adv. Funct. Mater.*, 2007, **17**, 605–612.
24 K. Möller, J. Kobler and T. Bein, *J. Mater. Chem.*, 2007, **17**, 624–631.
25 J. Kobler, K. Möller and T. Bein, *ACS Nano*, 2008, **2**, 791–799.
26 V. Cauda, A. Schlossbauer, J. Kecht, A. Zürner and T. Bein, *J. Am. Chem. Soc.*, 2009, **131**, 11361–11370.
27 Y. S. Lin, C. P. Tsai, H. Y. Huang, C. T. Kuo, Y. Hung, D. M. Huang, Y. C. Chen and C. Y. Mou, *Chem. Mater.*, 2005, **17**, 4570–4573.
28 F. Lu, S. H. Wu, Y. Hung and C. Y. Mou, *Small*, 2009, **5**, 1408–1413.
29 H. P. Lin and C. Y. Mou, *Acc. Chem. Res.*, 2002, **35**, 927–935.
30 T. Yokoi, Y. Sakamoto, O. Terasaki, Y. Kubota, T. Okubo and T. Tatsumi, *J. Am. Chem. Soc.*, 2006, **128**, 13664–13665.
31 T. Yokoi, J. Wakabayashi, Y. Otsuka, W. Fan, M. Iwama, R. Watanabe, K. Aramaki, A. Shimojima, T. Tatsumi and T. Okubo, *Chem. Mater.*, 2009, **21**, 3719–3729.
32 T. Yokoi, T. Karouji, S. Ohta, J. N. Kondo and T. Tatsumi, *Chem. Mater.*, 2010, **22**, 3900–3908.
33 R. Watanabe, T. Yokoi, E. Kobayashi, Y. Otsuka, A. Shimojima, T. Okubo and T. Tatsumi, *J. Colloid Interface Sci.*, 2011, **360**, 1–7.
34 C. Urata, Y. Aoyama, A. Tonegawa, Y. Yamauchi and K. Kuroda, *Chem. Commun.*, 2009, **45**, 5094–5096.
35 C. Urata, H. Yamada, R. Wakabayashi, Y. Aoyama, S. Hirosawa, S. Arai, S. Takeoka, Y. Yamauchi and K. Kuroda, *J. Am. Chem. Soc.*, 2011, **133**, 8102–8105.
36 H. Yamada, C. Urata, Y. Aoyama, S. Osada, Y. Yamauchi and K. Kuroda, *Chem. Mater.*, 2012, **24**, 1462–1471.
37 H. Yamada, C. Urata, H. Ujiie, Y. Yamauchi and K. Kuroda, *Nanoscale*, 2013, **5**, 6145–6153.
38 H. Yamada, C. Urata, S. Higashitamori, Y. Aoyama, Y. Yamauchi and K. Kuroda, *ACS Appl. Mater. Interfaces*, 2014, **6**, 3491–3500.
39 E. Yamamoto, M. Kitahara, T. Tsumura and K. Kuroda, *Chem. Mater.*, 2014, **26**, 2927–2933.
40 E. Yamamoto and K. Kuroda, *Bull. Chem. Soc. Jpn.*, 2016, **89**, 501–539.
41 S. H. Wu, Y. Hung and C. Y. Mou, *Chem. Commun.*, 2011, **47**, 9972–9985.
42 C. Argyo, V. Weiss, C. Bräuchle and T. Bein, *Chem. Mater.*, 2013, **26**, 435–451.
43 Y. Chen, H. Chen and J. Shi, *Adv. Mater.*, 2013, **25**, 3144–3176.
44 Z. Li, J. C. Barnes, A. Bosoy, J. F. Stoddart and J. I. Zink, *Chem. Soc. Rev.*, 2012, **41**, 2590–2605.

Open Access Article. Published on 16 April 2020. Downloaded on 2/9/2026 9:27:09 AM.
This article is licensed under a Creative Commons Attribution-NonCommercial 3.0 Unported Licence.

45 Y. S. Lin, K. R. Hurley and C. L. Haynes, *J. Phys. Chem. Lett.*, 2012, **3**, 364–374.
46 J. Lee, S. M. Kim and I. S. Lee, *Nano Today*, 2014, **9**, 631–667.
47 K. K. Coti, M. E. Belowich, M. Liong, M. W. Ambrogio, Y. A. Lau, H. A. Khatib, J. I. Zink, N. M. Khashab and J. F. Stoddart, *Nanoscale*, 2009, **1**, 16–39.
48 A. Popat, S. B. Hartono, F. Stahr, J. Liu, S. Z. Qiao and G. Qing Lu, *Nanoscale*, 2011, **3**, 2801–2808.
49 J. M. Rosenholm, C. Sahlgren and M. Linden, *Nanoscale*, 2010, **2**, 1870–1883.
50 K. Möller and T. Bein, *Chem. Mater.*, 2016, **29**, 371–388.
51 J. Peng, J. Liu, J. Liu, Y. Yang, C. Li and Q. Yang, *J. Mater. Chem. A*, 2014, **2**, 8118–8125.
52 S. M. Egger, K. R. Hurley, A. Datt, G. Swindlehurst and C. L. Haynes, *Chem. Mater.*, 2015, **27**, 3193–3196.
53 J. Fu, J. Jiao, H. Song, Z. Gu, Y. Liu, J. Geng, K. S. Jack, A. Du, J. Tang and C. Yu, *Chem. Mater.*, 2019, **32**, 341–347.
54 F. Yang, A. Skripka, M. S. Tabatabaei, S. H. Hong, F. Ren, Y. Huang, J. K. Oh, S. Martel, X. Liu, F. Vetrone and D. Ma, *Chem. Mater.*, 2019, **31**, 3201–3210.
55 X. Du and S. Z. Qiao, *Small*, 2015, **11**, 392–413.
56 X. Du and J. He, *Nanoscale*, 2011, **3**, 3984–4002.
57 Y. Wang, X. Du, Z. Liu, S. Shi and H. Lv, *J. Mater. Chem. A*, 2019, **7**, 5111–5152.
58 N. Z. Knezevic and J. O. Durand, *Nanoscale*, 2015, **7**, 2199–2209.
59 A. B. D. Nandiyanto, S. G. Kim, F. Iskandar and K. Okuyama, *Microporous Mesoporous Mater.*, 2009, **120**, 447–453.
60 H. Gustafsson, S. Isaksson, A. Altskar and K. Holmberg, *J. Colloid Interface Sci.*, 2016, **467**, 253–260.
61 L. Ernawati, R. Balgis, T. Ogi and K. Okuyama, *Langmuir*, 2017, **33**, 783–790.
62 V. Polshettiwar, D. Cha, X. Zhang and J. M. Basset, *Angew. Chem., Int. Ed.*, 2010, **49**, 9652–9656.
63 N. Bayal, B. Singh, R. Singh and V. Polshettiwar, *Sci. Rep.*, 2016, **6**, 24888.
64 A. Maity, A. Das, D. Sen, S. Mazumder and V. Polshettiwar, *Langmuir*, 2017, **33**, 13774–13782.
65 A. Maity and V. Polshettiwar, *ACS Appl. Nano Mater.*, 2018, **1**, 3636–3643.
66 E. Febriyanti, V. Suendo, R. R. Mukti, A. Prasetyo, A. F. Arifin, M. A. Akbar, S. Triwahyono, I. N. Marsih and Ismunandar, *Langmuir*, 2016, **32**, 5802–5811.
67 D. S. Moon and J. K. Lee, *Langmuir*, 2012, **28**, 12341–12347.
68 D. S. Moon and J. K. Lee, *Langmuir*, 2014, **30**, 15574–15580.
69 D. Shen, J. Yang, X. Li, L. Zhou, R. Zhang, W. Li, L. Chen, R. Wang, F. Zhang and D. Zhao, *Nano Lett.*, 2014, **14**, 923–932.
70 A. K. Meka, P. L. Abbaraju, H. Song, C. Xu, J. Zhang, H. Zhang, M. Yu and C. Yu, *Small*, 2016, **12**, 5169–5177.
71 C. Xu, M. Yu, O. Noonan, J. Zhang, H. Song, H. Zhang, C. Lei, Y. Niu, X. Huang, Y. Yang and C. Yu, *Small*, 2015, **11**, 5949–5955.
72 Y. Yang, Y. Niu, J. Zhang, A. K. Meka, H. Zhang, C. Xu, C. X. Lin, M. Yu and C. Yu, *Small*, 2015, **11**, 2743–2749.
73 H. Lin, K. Cui, Y. Yao, Q. Cai, Q. Feng and H. Li, *Chem. Lett.*, 2005, **34**, 918–919.
74 Q. Cai, Y. Geng, X. Zhao, K. Cui, Q. Sun, X. Chen, Q. Feng, H. Li and E. G. Vrieling, *Microporous Mesoporous Mater.*, 2008, **108**, 123–135.
75 X. Du, B. Shi, J. Liang, J. Bi, S. Dai and S. Z. Qiao, *Adv. Mater.*, 2013, **25**, 5981–5985.
76 X. Du and J. He, *Langmuir*, 2010, **26**, 10057–10062.
77 Y. Sheng and H. C. Zeng, *ACS Appl. Mater. Interfaces*, 2015, **7**, 13578–13589.
78 H. Yamada, H. Ujiie, C. Urata, E. Yamamoto, Y. Yamauchi and K. Kuroda, *Nanoscale*, 2015, **7**, 19557–19567.
79 E. Yamamoto, S. Mori, A. Shimojima, H. Wada and K. Kuroda, *Nanoscale*, 2017, **9**, 2464–2470.
80 Q. Liang, Q. Hu, G. Miao, B. Yuan and X. Chen, *Mater. Lett.*, 2015, **148**, 45–49.
81 Y. Min, K. Yang, Z. Liang, L. Zhang and Y. Zhang, *RSC Adv.*, 2015, **5**, 26269–26272.
82 S. W. Lim, H.-G. Jang, H.-I. Sim, C.-H. Shin, J.-H. Kim and G. Seo, *J. Porous Mater.*, 2014, **21**, 797–809.
83 A. Zhang, L. Gu, K. Hou, C. Dai, C. Song and X. Guo, *RSC Adv.*, 2015, **5**, 58355–58362.
84 H. Yang, S. Liao, C. Huang, L. Du, P. Chen, P. Huang, Z. Fu and Y. Li, *Appl. Surf. Sci.*, 2014, **314**, 7–14.
85 J. Shabir, C. Garkoti, Surabhi, D. Sah and S. Mozumdar, *Catal. Lett.*, 2018, **148**, 194–204.
86 H. Zhang, Z. Li, P. Xu, R. Wu and Z. Jiao, *Chem. Commun.*, 2010, **46**, 6783–6785.
87 S. Gai, P. Yang, P. Ma, L. Wang, C. Li, M. Zhang and L. Jun, *Dalton Trans.*, 2012, **41**, 4511–4516.
88 M. Dang, W. Li, Y. Zheng, X. Su, X. Ma, Y. Zhang, Q. Ni, J. Tao, J. Zhang, G. Lu, Z. Teng and L. Wang, *J. Mater. Chem. B*, 2017, **5**, 2625–2634.
89 L. Wu, Z. Jiao, M. Wu, T. Song and H. Zhang, *RSC Adv.*, 2016, **6**, 13303–13311.
90 D. Wang, X. Li, Z. Liu, X. Shi and G. Zhou, *Solid State Sci.*, 2017, **63**, 62–69.
91 C. Pereira, C. Alves, A. Monteiro, C. Magen, A. M. Pereira, A. Ibarra, M. R. Ibarra, P. B. Tavares, J. P. Araujo, G. Blanco, J. M. Pintado, A. P. Carvalho, J. Pires, M. F. Pereira and C. Freire, *ACS Appl. Mater. Interfaces*, 2011, **3**, 2289–2299.
92 A. J. Paula, L. A. Montoro, A. G. Filho and O. L. Alves, *Chem. Commun.*, 2012, **48**, 591–593.
93 M. Wu, Q. Meng, Y. Chen, Y. Du, L. Zhang, Y. Li, L. Zhang and J. Shi, *Adv. Mater.*, 2015, **27**, 215–222.
94 F. Gai, T. Zhou, G. Chu, Y. Li, Y. Liu, Q. Huo and F. Akhtar, *Dalton Trans.*, 2016, **45**, 508–514.
95 K. Zhang, L. L. Xu, J. G. Jiang, N. Calin, K. F. Lam, S. J. Zhang, H. H. Wu, G. D. Wu, B. Albela, L. Bonneviot and P. Wu, *J. Am. Chem. Soc.*, 2013, **135**, 2427–2430.
96 Y. J. Yu, J. L. Xing, J. L. Pang, S. H. Jiang, K. F. Lam, T. Q. Yang, Q. S. Xue, K. Zhang and P. Wu, *ACS Appl. Mater. Interfaces*, 2014, **6**, 22655–22665.
97 J. Jiao, J. Fu, Y. Wei, Z. Zhao, A. Duan, C. Xu, J. Li, H. Song, P. Zheng, X. Wang, Y. Yang and Y. Liu, *J. Catal.*, 2017, **356**, 269–282.

 This journal is © The Royal Society of Chemistry 2020

Open Access Article. Published on 16 April 2020. Downloaded on 2/9/2026 9:27:09 AM.
This article is licensed under a Creative Commons Attribution-NonCommercial 3.0 Unported Licence.

98 M. Kalantari, Y. Liu, E. Strounina, Y. Yang, H. Song and C. Yu, *J. Mater. Chem. A*, 2018, **6**, 17579–17586.
99 Y. Wang, Y. A. Nor, H. Song, Y. Yang, C. Xu, M. Yu and C. Yu, *J. Mater. Chem. B*, 2016, **4**, 2646–2653.
100 Y. Wang, H. Song, Y. Yang, Y. Liu, J. Tang and C. Yu, *Chem. Mater.*, 2018, **30**, 5770–5776.
101 Y. Wang, H. Song, M. Yu, C. Xu, Y. Liu, J. Tang, Y. Yang and C. Yu, *J. Mater. Chem. B*, 2018, **6**, 4089–4095.
102 M. Huang, L. Liu, S. Wang, H. Zhu, D. Wu, Z. Yu and S. Zhou, *Langmuir*, 2017, **33**, 519–526.
103 Y. Shi, J. Fu and Y. Yang, *Microporous Mesoporous Mater.*, 2020, **294**, 109914.
104 A. Monnier, F. Schuth, Q. Huo, D. Kumar, D. Margolese, R. S. Maxwell, G. D. Stucky, M. Krishnamurty, P. Petroff, A. Firouzi, M. Janicke and B. F. Chmelka, *Science*, 1993, **261**, 1299–1303.
105 S. Schacht, Q. Huo, I. G. Voigt-Martin, G. D. Stucky and F. Schiith, *Science*, 1996, **273**, 768–771.
106 P. Feng, X. Bu, G. D. Stucky and D. J. Pine, *J. Am. Chem. Soc.*, 2000, **122**, 994–995.
107 D. Volkmer, S. Tugulu, M. Fricke and T. Nielsen, *Angew. Chem., Int. Ed.*, 2003, **42**, 58–61.
108 K. Cui, Q. Cai, X. H. Chen, Q. L. Feng and H. D. Li, *Microporous Mesoporous Mater.*, 2004, **68**, 61–64.
109 H. Chen, J. He, H. Tang and C. Yan, *Chem. Mater.*, 2008, **20**, 5894–5900.
110 Z. Yi, L. F. Dumee, C. J. Garvey, C. Feng, F. She, J. E. Rookes, S. Mudie, D. M. Cahill and L. Kong, *Langmuir*, 2015, **31**, 8478–8487.
111 B. Q. Shan, J. L. Xing, T. Q. Yang, B. Peng, P. Hao, Y. X. Zong, X. Q. Chen, Q. S. Xue, K. Zhang and P. Wu, *CrystEngComm*, 2019, **21**, 4030–4035.
112 D. Yi, Q. Zhang, Y. Liu, J. Song, Y. Tang, F. Caruso and Y. Wang, *Angew. Chem., Int. Ed.*, 2016, **55**, 14733–14737.
113 A. Kuijk, A. van Blaaderen and A. Imhof, *J. Am. Chem. Soc.*, 2011, **133**, 2346–2349.
114 D. Yi, C. Xu, R. Tang, X. Zhang, F. Caruso and Y. Wang, *Angew. Chem., Int. Ed.*, 2016, **55**, 8375–8380.
115 C. Deng, Q. Zhang, C. Fu, F. Zhou, W. Yang, D. Yi, X. Wang, Y. Tang, F. Caruso and Y. Wang, *Chem. Mater.*, 2019, **31**, 4291–4298.
116 K. Zhang, B. n. Albela, M. Y. He, Y. Wang and L. Bonneviot, *Phys. Chem. Chem. Phys.*, 2009, **11**, 2912–2921.
117 K. Zhang, K. F. Lam, B. Albela, T. Xue, L. Khrouz, Q. W. Hou, E. H. Yuan, M. Y. He and L. Bonneviot, *Chem.–Eur. J.*, 2011, **17**, 14258–14266.
118 K. Zhang, Y. Zhang, Q.-W. Hou, E.-H. Yuan, J.-G. Jiang, B. Albela, M.-Y. He and L. Bonneviot, *Microporous Mesoporous Mater.*, 2011, **143**, 401–405.
119 K. Zhang, H.-L. Chen, B. Albela, J.-G. Jiang, Y.-M. Wang, M.-Y. He and L. Bonneviot, *Eur. J. Inorg. Chem.*, 2011, **2011**, 59–67.
120 K. Zhang, E.-H. Yuan, L.-L. Xu, Q.-S. Xue, C. Luo, B. Albela and L. Bonneviot, *Eur. J. Inorg. Chem.*, 2012, **2012**, 4183–4189.
121 X. Meng and F. S. Xiao, *Chem. Rev.*, 2014, **114**, 1521–1543.
122 P. C. Liu, Y. J. Yu, B. Peng, S. Y. Ma, T. Y. Ning, B. Q. Shan, T. Q. Yang, Q. S. Xue, K. Zhang and P. Wu, *Green Chem.*, 2017, **19**, 5575–5581.
123 W. Stöber and A. Fink, *J. Colloid Interface Sci.*, 1968, **26**, 62–69.
124 K. Ma, Y. Gong, T. Aubert, M. Z. Turker, T. Kao, P. C. Doerschuk and U. Wiesner, *Nature*, 2018, **558**, 577–580.
125 T. Zhao, A. Elzatahry, X. Li and D. Zhao, *Nat. Rev. Mater.*, 2019, **4**, 775–791.
126 F. Gao, R. Sougrat, B. Albela and L. Bonneviot, *J. Phys. Chem. C*, 2011, **115**, 7285–7291.
127 Y. Yang, S. Bernardi, H. Song, J. Zhang, M. Yu, J. C. Reid, E. Strounina, D. J. Searles and C. Yu, *Chem. Mater.*, 2016, **28**, 704–707.
128 B. Peng, Y.-X. Zong, M.-Z. Nie, B.-Q. Shan, T.-Q. Yang, P. Hao, S.-Y. Ma, K.-F. Lam and K. Zhang, *New J. Chem.*, 2019, **43**, 15777–15784.
129 M. Griin, I. Lauer and K. K. Unge, *Adv. Mater.*, 1997, **9**, 254–257.
130 T. N. Zemb, M. Klossek, T. Lopian, J. Marcus, S. Schöettl, D. Horinek, S. F. Prevost, D. Touraud, O. Diat, S. Marcelja and W. Kunz, *Proc. Natl. Acad. Sci. U. S. A.*, 2016, **113**, 4260–4265.
131 B. A. Keiser, D. Varié, R. E. Barden and S. L. Holt, *J. Phys. Chem.*, 1979, **83**, 1276–1280.
132 G. D. Smith, C. E. Donelan and R. E. Barden, *J. Colloid Interface Sci.*, 1976, **60**, 488–496.
133 S. Schöttl, J. Marcus, O. Diat, D. Touraud, W. Kunz, T. Zemb and D. Horinek, *Chem. Sci.*, 2014, **5**, 2949–2954.
134 Y. Liu, J. Xu, H. Deng, J. Song and W. Hou, *RSC Adv.*, 2018, **8**, 1371–1377.
135 Z. Chen, B. Peng, J. Q. Xu, X. C. Xiang, D. F. Ren, T. Q. Yang, S. Y. Ma, K. Zhang and Q. M. Chen, *Nanoscale*, 2020, **12**, 3657–3662.
136 A. Maity and V. Polshettiwar, *ChemSusChem*, 2017, **10**, 3866–3913.
137 C. Xu, C. Lei and C. Yu, *Front. Chem.*, 2019, **7**, 290.
138 V. Polshettiwar, J. Thivolle-Cazat, M. Taoufik, F. Stoffelbach, S. Norsic and J. M. Basset, *Angew. Chem., Int. Ed.*, 2011, **50**, 2747–2751.
139 A. Fihri, M. Bouhrara, U. Patil, D. Cha, Y. Saih and V. Polshettiwar, *ACS Catal.*, 2012, **2**, 1425–1431.
140 A. Fihri, D. Cha, M. Bouhrara, N. Almana and V. Polshettiwar, *ChemSusChem*, 2012, **5**, 85–89.
141 H. Peng, D. Wang, L. Xu and P. Wu, *Chin. J. Catal.*, 2013, **34**, 2057–2065.
142 H. Yang, S. Li, X. Zhang, X. Wang and J. Ma, *J. Mater. Chem. A*, 2014, **2**, 12060–12067.
143 M. Dhiman, B. Chalke and V. Polshettiwar, *ACS Sustainable Chem. Eng.*, 2015, **3**, 3224–3230.
144 Z. S. Qureshi, P. B. Sarawade, M. Albert, V. D'Elia, M. N. Hedhili, K. Köhler and J.-M. Basset, *ChemCatChem*, 2015, **7**, 635–642.
145 S. Schünemann, G. Dodekatos and H. Tüysüz, *Chem. Mater.*, 2015, **27**, 7743–7750.

Open Access Article. Published on 16 April 2020. Downloaded on 2/9/2026 9:27:09 AM.
This article is licensed under a Creative Commons Attribution-NonCommercial 3.0 Unported Licence.

146 D. Jung, Y.-J. Kim and J.-K. Lee, *Bull. Korean Chem. Soc.*, 2016, **37**, 386–389.
147 R. Singh, R. Bapat, L. Qin, H. Feng and V. Polshettiwar, *ACS Catal.*, 2016, **6**, 2770–2784.
148 X. Deng, R. Rin, J.-C. Tseng, C. Weidenthaler, U.-P. Apfel and H. Tüysüz, *ChemCatChem*, 2017, **9**, 4238–4243.
149 M. Dhiman, B. Chalkeb and V. Polshettiwar, *J. Mater. Chem. A*, 2017, **5**, 1935–1940.
150 J. Xu, J. Zhang, H. Peng, X. Xu, W. Liu, Z. Wang, N. Zhang and X. Wang, *Microporous Mesoporous Mater.*, 2017, **242**, 90–98.
151 T.-Q. Yang, T.-Y. Ning, B. Peng, B.-Q. Shan, Y.-X. Zong, P. Hao, E.-H. Yuan, Q.-M. Chen and K. Zhang, *Catal. Sci. Technol.*, 2019, **9**, 5786–5792.
152 Y. Choi, Y. S. Yun, H. Park, D. S. Park, D. Yun and J. Yi, *Chem. Commun.*, 2014, **50**, 7652–7655.
153 S. Afzal, X. Quan, S. Chen, J. Wang and D. Muhammad, *J. Hazard. Mater.*, 2016, **318**, 308–318.
154 Z. N. Siddiqui, K. Khan and N. Ahmed, *Catal. Lett.*, 2014, **144**, 623–632.
155 M. Bouhrara, C. Ranga, A. Fihri, R. R. Shaikh, P. Sarawade, A.-H. Emwas, M. N. Hedhili and V. Polshettiwar, *ACS Sustainable Chem. Eng.*, 2013, **1**, 1192–1199.
156 S. M. Sadeghzadeh, *Green Chem.*, 2015, **17**, 3059–3066.
157 M. Wu, L. Kong, K. Wang, R. Jin, T. Cheng and G. Liu, *Catal. Sci. Technol.*, 2015, **5**, 1750–1757.
158 S. M. Sadeghzadeh, R. Zhiani, M. Khoobi and S. Emrani, *Microporous Mesoporous Mater.*, 2018, **257**, 147–153.
159 T. Q. Yang, B. Peng, B. Q. Shan, Y. X. Zong, J. G. Jiang, P. Wu and K. Zhang, *Nanomaterials*, 2020, **10**, 261.
160 H. Peng, X. Zhang, X. Han, X. You, S. Lin, H. Chen, W. Liu, X. Wang, N. Zhang, Z. Wang, P. Wu, H. Zhu and S. Dai, *ACS Catal.*, 2019, **9**, 9072–9080.
161 M. A. Boles, D. Ling, T. Hyeon and D. V. Talapin, *Nat. Mater.*, 2016, **15**, 141–153.
162 L. A. Peyser, A. E. Vinson, A. P. Bartko and R. M. Dickson, *Science*, 2001, **291**, 103–106.
163 J. Zheng, P. R. Nicovich and R. M. Dickson, *Annu. Rev. Phys. Chem.*, 2007, **58**, 409–431.
164 S. N. Baker and G. A. Baker, *Angew. Chem., Int. Ed.*, 2010, **49**, 6726–6744.
165 Y. Zong, T. Yang, P. Hao, B. Shan, B. Peng, X. Hu, R. Tao, X. Chen, P. Wu and K. Zhang, *Microporous Mesoporous Mater.*, 2020, 110229, DOI: 10.1016/j.micromeso.2020.110229.
166 J. Liu, P. N. Duchesne, M. Yu, X. Jiang, X. Ning, R. D. Vinluan III, P. Zhang and J. Zheng, *Angew. Chem., Int. Ed.*, 2016, **55**, 8894–8898.
167 Z. Wu and R. Jin, *Nano Lett.*, 2010, **10**, 2568–2573.
168 J. Zheng, C. Zhou, M. Yu and J. Liu, *Nanoscale*, 2012, **4**, 4073–4083.
169 Y. Chen, T. Yang, H. Pan, Y. Yuan, L. Chen, M. Liu, K. Zhang, S. Zhang, P. Wu and J. Xu, *J. Am. Chem. Soc.*, 2014, **136**, 1686–1689.
170 T. Yang, S. Dai, S. Yang, L. Chen, P. Liu, K. Dong, J. Zhou, Y. Chen, H. Pan, S. Zhang, J. Chen, K. Zhang, P. Wu and J. Xu, *J. Phys. Chem. Lett.*, 2017, **8**, 3980–3985.
171 S. E. Crawford, C. M. Andolina, A. M. Smith, L. E. Marbella, K. A. Johnston, P. J. Straney, M. J. Hartmann and J. E. Millstone, *J. Am. Chem. Soc.*, 2015, **137**, 14423–14429.
172 C. Yi, H. Zheng, P. J. Herbert, Y. Chen, R. Jin and K. L. Knappenberger, *J. Phys. Chem. C*, 2017, **121**, 24894–24902.
173 G. Wang, T. Huang, R. W. Murray, L. Menard and R. G. Nuzzo, *J. Am. Chem. Soc.*, 2004, **127**, 812–813.
174 T. Yang, S. Dai, H. Tan, Y. Zong, Y. Liu, J. Chen, K. Zhang, P. Wu, S. Zhang, J. Xu and Y. Tian, *J. Phys. Chem. C*, 2019, **123**, 18638–18645.
175 T. Yang, B. Shan, F. Huang, S. Yang, B. Peng, E. Yuan, P. Wu and K. Zhang, *Commun. Chem.*, 2019, **2**, 132.

This journal is © The Royal Society of Chemistry 2020